Article

Neuron

Morning and Evening Circadian Pacemakers Independently Drive Premotor Centers via a Specific Dopamine Relay

Highlights

- The *Drosophila* circadian pacemaker network promotes rhythmic daily activity
- EB ring neurons (EB-RNs) exhibit spontaneous morning and evening activity peaks
- The two EB-RN peaks are independently driven by M and E circadian pacemakers
- Both M and E pacemakers regulate EB-RN activity via specific dopamine interneurons

Authors

Xitong Liang, Margaret C.W. Ho, Yajun Zhang, Yulong Li, Mark N. Wu, Timothy E. Holy, Paul H. Taghert

Correspondence

taghertp@wustl.edu

In Brief

Liang et al. describe neural outputs from the *Drosophila* circadian pacemaker network regulating locomotor rhythms: via a specific dopamine relay, the network forms parallel connections to the central complex, the pre-motor area dictating the balance between rest and activity.

Liang et al., 2019, Neuron *102*, 843–857
May 22, 2019
https://doi.org/10.1016/j.neuron.2019.03.028

CellPress

Neuron
Article

Morning and Evening Circadian Pacemakers Independently Drive Premotor Centers via a Specific Dopamine Relay

Xitong Liang,[1,7] Margaret C.W. Ho,[2] Yajun Zhang,[3,4,5] Yulong Li,[3,4,5,6] Mark N. Wu,[2] Timothy E. Holy,[1] and Paul H. Taghert[1,8,*]
[1]Department of Neuroscience, Washington University in St. Louis, St. Louis, MO 63110, USA
[2]Department of Neurology, Johns Hopkins University School of Medicine, Baltimore, MD 21205, USA
[3]State Key Laboratory of Membrane Biology, Peking University School of Life Sciences, Beijing 100871, China
[4]Peking-Tsinghua Center for Life Sciences, Academy for Advanced Interdisciplinary Studies, Peking University, Beijing 100871, China
[5]PKU-IDG/McGovern Institute for Brain Research, Beijing 100871, China
[6]Chinese Institute for Brain Research, Beijing 100871, China
[7]Present address: Max Planck Institute for Brain Research, 60438 Frankfurt am Main, Germany
[8]Lead Contact
*Correspondence: taghertp@wustl.edu
https://doi.org/10.1016/j.neuron.2019.03.028

SUMMARY

Many animals exhibit morning and evening peaks of locomotor behavior. In *Drosophila*, two corresponding circadian neural oscillators—M (morning) cells and E (evening) cells—exhibit a corresponding morning or evening neural activity peak. Yet we know little of the neural circuitry by which distinct circadian oscillators produce specific outputs to precisely control behavioral episodes. Here, we show that ring neurons of the ellipsoid body (EB-RNs) display spontaneous morning and evening neural activity peaks *in vivo*: these peaks coincide with the bouts of locomotor activity and result from independent activation by M and E pacemakers. Further, M and E cells regulate EB-RNs via identified PPM3 dopaminergic neurons, which project to the EB and are normally co-active with EB-RNs. These *in vivo* findings establish the fundamental elements of a circadian neuronal output pathway: distinct circadian oscillators independently drive a common pre-motor center through the agency of specific dopaminergic interneurons.

INTRODUCTION

Circadian rhythms provide adaptive value by promoting expression of diverse physiological processes and behaviors at specific times of the day. In mammals, rhythms in hormone release, rest/activity cycles, body temperature, and metabolism are all controlled by the multi-oscillator system of pacemakers in the suprachiasmatic nucleus (SCN) of the anterior hypothalamus. Numerous studies have documented that the SCN uses hormonal and neuronal signaling to provide adaptive phasic information across all times of day (Lehman et al., 1987; Moore and Klein, 1974; Ralph et al., 1990; de la Iglesia et al., 2003; Kalsbeek et al., 2006; VanderLeest et al., 2007). However, the information connecting SCN signaling to neural circuits that translate its outputs is fragmentary. Lacking direct *in vivo* experimental observations, the definition of circadian output networks remains a significant challenge.

In *Drosophila*, a prominent circadian output is the daily locomotor activity rhythm, which peaks once around dawn and again around dusk (Figure 1B). The rhythm is controlled by molecular clocks that cycle synchronously within ~150 circadian pacemaker neurons (Nitabach and Taghert, 2008). Among these circadian neurons, two separate groups (termed M cells and E cells) control the morning (M) and evening (E) activity peaks (Stoleru et al., 2004; Grima et al., 2004; Yoshii et al., 2004). Previously, we reported that different groups of circadian neurons display rhythmic but asynchronous circadian neural activity *in vivo*: they peak at different yet stereotyped times of day (Liang et al., 2016). These neural activity rhythms depend on their synchronous molecular clocks, but their activity peak times are staggered by neuropeptide-mediated interactions between circadian neuron groups. This allows the network to create multiple phasic time points (Liang et al., 2017). Consequently, M cells peak in the morning and E cells peak in the evening. The distinct peak times of M cells and E cells could potentially guide output motor circuits to generate independent morning and evening locomotor behavioral peaks. To support this emerging network view of pacemaker-regulated behavior, we wished to ask which pre-motor centers transduce circadian timing signals to generate morning or evening phase-specific locomotor activity. As a strategy, we reasoned that spontaneous neural activity patterns corresponding to the daily bimodal activity pattern could help identify the critical pre-motor elements.

Robie et al. (2017) performed an unbiased screen of sparsely labeled neuronal groups to determine which, when activated, could initiate locomotor activity. By this analysis, the strongest candidates were the ring neurons of the ellipsoid body (EB-RNs) (Figure 1A). In parallel, silencing these same EB-RNs

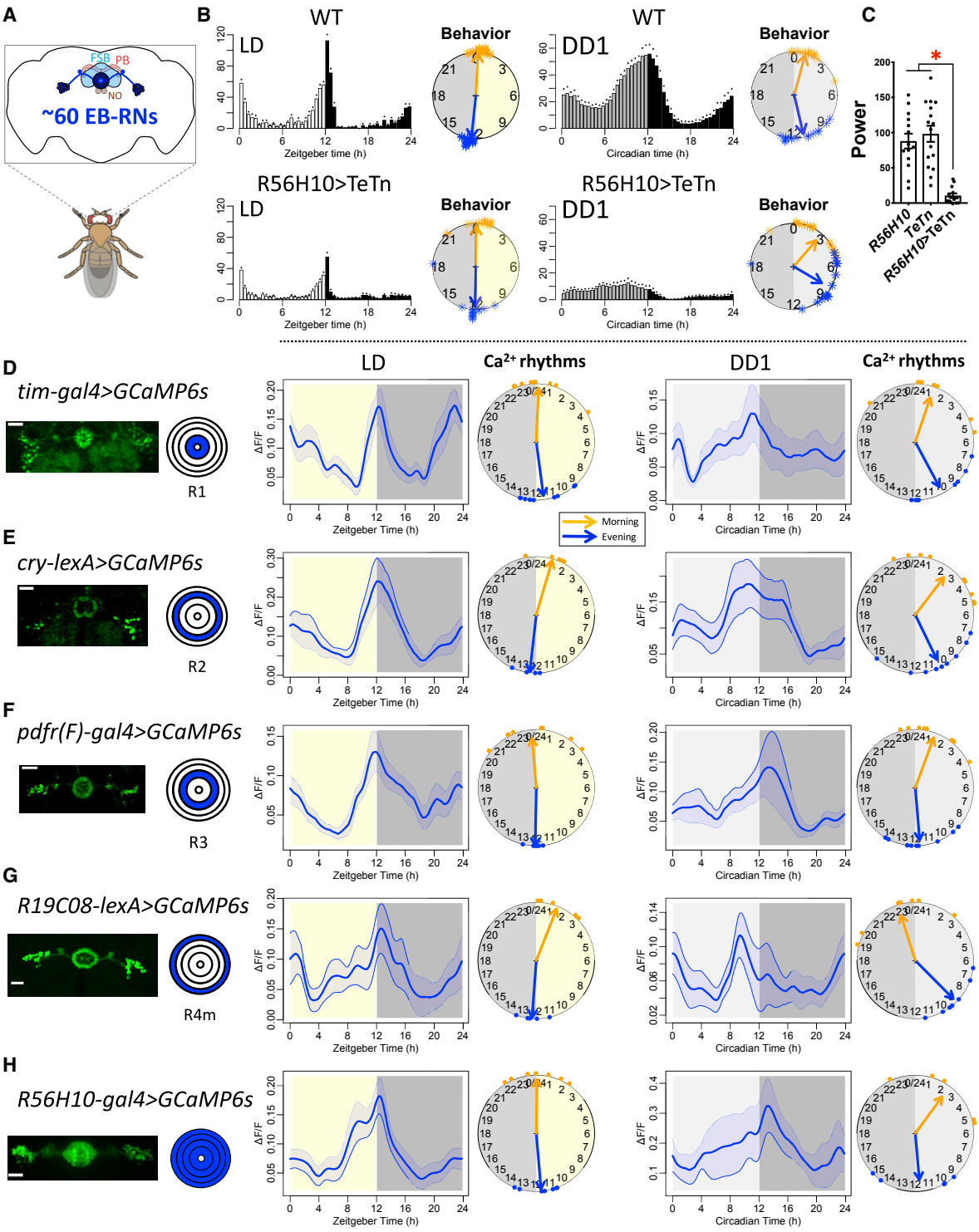

Figure 1. Daily Bimodal Neural Activity Patterns of EB Ring Neurons

(A) The central complex in the fly brain. EB-RNs, ellipsoid body ring neurons; FSB, fan-shaped body; PB, protocerebral bridge; NO, noduli.

(B) The average locomotor activity histogram and phase distributions of behavioral peaks of wild-type *R56H10-GAL4/GCaMP6s* flies (above, n = 16) and flies in which EB-RNs are silenced by TeTn (below, n = 14). Both genotypes are shown under a 12-h light to 12-h dark (LD) cycle (left) and in the first day under constant darkness (DD) (right). Dots indicate SEM.

(C) Average rhythm strength (power) of locomotor activity for 9 days under DD displayed by two genetic controls and by flies in which EB-RNs express TeTn; asterisk denotes significant differences compared to control ($p < 0.0001$, Mann-Whitney test).

(legend continued on next page)

reduced spontaneous locomotor activity (Martín-Peña et al., 2014). EB-RNs are a subset of neurons that constitute the central complex, the primary locomotor control center in insects (Strauss and Heisenberg, 1993; Pfeiffer and Homberg, 2014). EB-RNs encode visual landmarks for visuospatial-memory-based orientation and navigation (Neuser et al., 2008; Ofstad et al., 2011; Seelig and Jayaraman, 2013). In the monarch butterfly, EB-RNs are involved in sun-compass navigation (Heinze and Reppert, 2011), which requires timing information from circadian clocks (Froy et al., 2003). Several recent studies have linked activity in subsets of the EB-RN to the regulation of sleep-wake physiology. Liu et al. (2016) identified an EB subset whose activity defines an integrator that promotes sleep drive. In addition, two independent groups described synaptic links between a subset of the DN1 group of circadian pacemakers to subgroups of EB-RNs (Lamaze et al., 2018; Guo et al., 2018), which may help regulate sleep/arousal. DN1 cells integrate outputs from M and E cells and regulate both locomotor activity and sleep (Zhang et al., 2010; Liang et al., 2017; Guo et al., 2016). Therefore, we measured spontaneous activity in EB-RNs *in vivo* first, to see whether they represent a point of convergent circadian regulation that could lead to daily bouts of locomotor activity.

RESULTS

Spontaneous Daily Bimodal Activity in EB-RNs *In Vivo*

To test whether EB-RNs regulate circadian locomotor activity, we expressed tetanus toxin light chain (TeTn, Sweeney et al., 1995) to block neurotransmission in the majority of ~60 EB-RNs. As expected, the circadian rhythm of locomotor activity in these flies was impaired under constant darkness (DD), as was the general level of activity (Figures 1B, 1C, and Table S1). Then, to learn about the possible involvement of the EB-RNs in normal rhythmic locomotion, we measured *in vivo* spontaneous activity exhibited by these neurons in otherwise wild-type flies. Using the genetically encoded calcium sensor GCaMP6s (Chen et al., 2013), we performed *in vivo* Ca^{2+} imaging in living flies for 24 h using methods previously described (Liang et al., 2016, 2017). EB-RNs contain several genetically and morphologically distinct subgroups (Renn et al., 1999a). We dissected four EB-RN subgroups using different genetic drivers that use regulatory sequences associated with different circadian clock-related genes: one with sequences from *timeless*, one from *cryptochrome*, and two from *pdfr* (*pigment-dispersing factor receptor*) (Figures 1D–1G and S1A). In both 12-h light to 12-h dark (LD) cycles and in DD conditions, the four different EB-RN subgroups we tested displayed spontaneous, daily Ca^{2+} rhythms (Figures 1D–1G and Figures S2A–S2D). These dynamic signals were not a consequence of rhythmic GCaMP6 sensor expression (Figures S3A–S3F). The average Ca^{2+} activity profile of each subgroup was bimodal (Hartigans' dip test, LD: $p < 0.0001$, DD: $p < 0.05$), with a peak around dawn and another around dusk. At these two peaks, with high-frequency-light-sheet imaging (1 Hz), we found that many EB-RNs showed an increase in the incidence and magnitude of fast spontaneous activity events (Figure S3G). The two daily peaks corresponded to the times of day when flies showed daily locomotor activity peaks (Figure 1B). The outer subgroup of EB-RNs caused the strongest effects on locomotor activity, according to Robie et al. (2017). We tested the same split-GAL4 drivers as reported by Robie et al. (2017) and found that these locomotion-promoting EB-RNs likewise displayed a similar spontaneous daily bimodal activity pattern (Figure S1B; Hartigans' dip test, $p < 0.0001$). We also confirmed the daily bimodal activity pattern exhibited by different EB-RN subgroups using a separate, circadian-clock-irrelevant driver line to label the majority of EB-RNs (Figures 1H and S2E; Hartigans' dip test, LD: $p < 0.001$, DD: $p < 0.01$).

To test the correlation between EB-RN neural activity and locomotor activity in single flies in our experimental paradigm directly, we performed *in vivo* 24-h Ca^{2+} imaging while simultaneously measuring spontaneous leg movements as a proxy for locomotor activity levels (Figure 2A). EB-RN activity was strongly correlated with such behavioral activity in individual flies, both at a daily timescale (Figures 2F–2K) and at a shorter (hourly) timescale (Figures 2C–2E and S4E–S4L). Analysis of the shorter timescale indicated that increases in EB-RN activity were coincident with increases in behavioral activity; decreases typically preceded decreases in behavioral activity by a few minutes (Figure 2E). We noted that, under DD, the imaged flies (Figure 2F) showed higher locomotor activity around the middle of subjective day than did freely moving flies (Figure 1B, right panel). The increase in activity during the middle of the subjective day was not caused by illumination of the specimen during imaging (Figures S4A–S4C) and was not observed under LD conditions. Under LD, both the locomotor activity and EB-RN activity clearly showed two daily peaks. Thus, EB-RNs, consistent with their documented roles as pre-motor activity centers, exhibit spontaneous daily neural activity rhythms that precisely correspond to the pattern of circadian locomotor rhythms.

Circadian Pacemaker Neurons Drive EB-RN Activity Rhythms

The daily neural activity rhythms in EB-RNs could reflect rhythmic sensory inputs, either proprioceptive or visual. For example, recent studies suggest that EB-RNs encode self-motion information (Shiozaki and Kazama, 2017). Therefore, to block ascending proprioceptive sensory inputs, we transected connectives between the brain and ventral nerve cord (between subesophageal and first thoracic neuromeres) immediately before Ca^{2+} imaging. EB-RNs still displayed normal bimodal activity rhythms (Figure 3A). These EB-RN rhythms persisted even when the entire body of the fly was removed immediately before imaging (Figure 3B). Therefore, spontaneous bimodal EB-RN

(D–H) Daily Ca^{2+} activity patterns of the EB ring neuron subgroups: (D) R1 labeled by *tim-GAL4*, (E) R2 labeled by *cry-lexA*, (F) R3 labeled by *pdfr(F)-GAL4*, (G) R4 labeled by *R19H08(pdfr)-lexA*, and (H) R1-4 labeled by *R56H10-GAL4*. Left, confocal images of EB ring neurons and diagrams of their concentric arborizations; scale bars, 25 μm. Middle and right, average Ca^{2+} transients and Ca^{2+} phase distributions for both morning peaks (orange dots and arrow) and evening peaks (blue dots and arrow). Middle, under LD; Right, under DD.

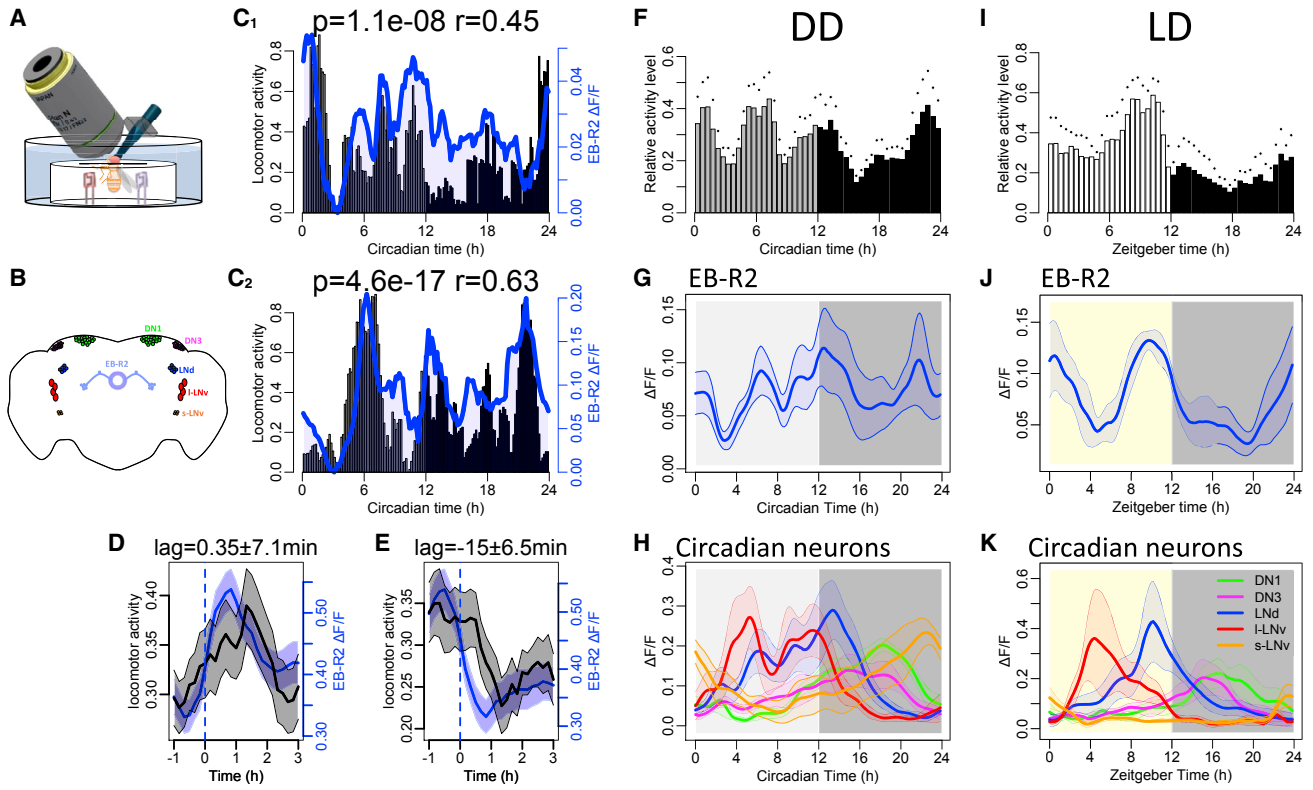

Figure 2. EB Ring Neuron Activity Is Correlated with Locomotor Activity

(A) Illustration of long-term *in vivo* imaging arrangement combined with infrared measurement of locomotor activity (see Methods).

(B) Map of the major circadian neuron groups and EB ring neurons.

(C) Representative recordings of two flies in DD for 24 h: bars, normalized locomotor activity counts per 10 m; blue traces, Ca^{2+} activity of EB-R2 neurons in the same fly.

(D and E) Average locomotor activity (black) and Ca^{2+} activity of EB-R2 neurons (blue) aligned by (D) increasing phase and (E) decreasing phase of Ca^{2+} activity. The averaged phase lags were calculated by cross-correlation: (D) 0.35 ± 7 min; (E) −15 ± 0.5 min.

(F–H) Average locomotor activity (F) and average Ca^{2+} transients of (G) EB-R2 neurons and (H) circadian pacemaker neurons in the same flies (*cry-lexA>GCaMP6s*; n = 6 flies) during DD1. Dots and shading indicate SEM.

(I–K) Average locomotor activity (I) and average Ca^{2+} transients of (J) EB-R2 neurons and (K) circadian pacemaker neurons in the same flies (*cry-lexA>GCaMP6s*; n = 5 flies) under LD cycles.

activity rhythms are not a consequence of locomotor behavioral activity. Previous studies also showed that EB-RNs receive large-scale visual inputs (Seelig and Jayaraman, 2013; Omoto et al., 2017; Sun et al., 2017). Therefore, we removed visual inputs by testing flies in DD (Figure 1) or by testing genetically blind *norpA*^{P24} mutant flies (Figure 3C): in both cases, normal EB-RN activity rhythms persisted. Together, these results indicate that neither visual nor proprioceptive inputs are necessary for spontaneous EB-RN activity rhythms.

To determine whether EB-RN activity rhythms are driven by molecular clocks, we measured Ca^{2+} activity in circadian-defective *per*^{01} (null) mutant flies (Konopka and Benzer, 1971), which fail to display circadian clock-dependent anticipatory behavior. Although *per*^{01} flies still had two peaks of startle responses (to the lights-on and lights-off stimuli under LD cycles), daily Ca^{2+} activity patterns in EB-RNs were arrhythmic (Figure 3D). Therefore, EB-RN activity rhythms specifically correlate with—and entirely depend on—circadian clock signals that regulate daily behavioral peaks. Notably, EB-RNs do not exhibit measurable expression of the core clock gene *period*, which is highly expressed and cycles in circadian pacemaker neurons (Figure S1C) (Kaneko and Hall, 2000). Furthermore, manipulations that alter the pace of circadian clocks in a subset of circadian neurons shifted the phase of locomotor activity phases, as previously reported (Stoleru et al., 2005; Yao and Shafer, 2014), while the same manipulation within EB-RNs did not affect locomotor behavior (Figures S1D–S1F). Thus, we conclude that daily EB-RN activity rhythms are downstream of circadian timing information provided by circadian pacemaker neurons. To test whether circadian neurons regulate EB-RNs, we impaired a crucial signal within the pacemaker network, the neuropeptide PDF (Renn et al., 1999b). In PDF receptor mutant (*pdfr*^{han5304}) flies (Hyun et al., 2005), the EB-RNs' activity pattern under LD transformed to a daily unimodal one (Hartigans' dip test, p = 0.23): the morning activity peak was lost, and the evening peak was advanced (Figure 3E; Watson-Williams test, p = 0.00012). This neural

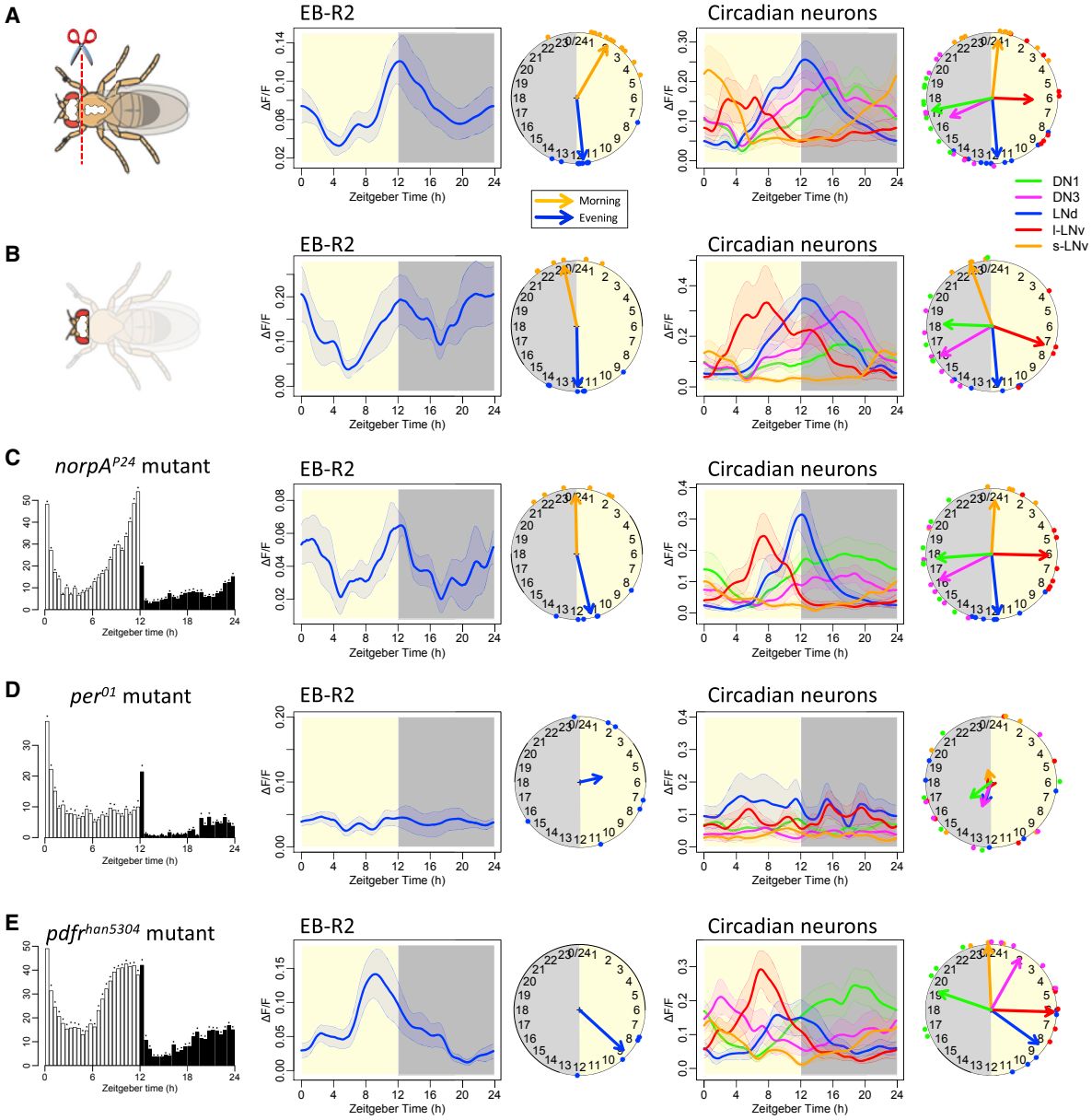

Figure 3. EB Ring Neuron Rhythms Are Driven by Clocks, Not in Response to Behavior or Sensation

(A) Daily Ca^{2+} activity patterns of (middle) EB-R2 neurons and (right) circadian neurons under LD immediately after cutting the neural connectives between brain and ventral nerve cord in otherwise intact flies (dotted line indicates level of the cut; n = 10 flies).

(B) Daily Ca^{2+} activity patterns of EB-R2 and circadian neurons under LD immediately after transecting the connection between heads and bodies, then removing the bodies (n = 6 flies).

(C) In blind *cry-lexA>GCaMP6s* flies (*norpA^{P24}* mutant), (left) average locomotor activity (n = 22 flies) and daily Ca^{2+} activity patterns (middle) of EB-R2 neurons and (right) circadian neurons under LD (n = 6 flies).

(D) In arrhythmic *cry-lexA>GCaMP6s* flies (*per^{01}* mutants), average locomotor activity (n = 16 flies) and arrhythmic Ca^{2+} activity patterns of EB-R2 and of circadian neurons under LD (n = 7 flies).

(E) In Pdfr-deficient *cry-lexA>GCaMP6s* flies (*pdfr^{han5304}* mutants), average locomotor activity (n = 8 flies) and Ca^{2+} activity patterns of EB-R2 and of circadian neurons under LD (n = 7 flies).

activity pattern mirrors the changes in locomotor activity pattern typically displayed by *pdfr^{han5304}* flies. Meanwhile, EB-RNs responded to thermogenetic and pharmacogenetic activation of PDF-releasing neurons (Figures S5A and S5B). Thus, EB-RN activity rhythms could be driven (directly or indirectly) by PDF-expressing circadian pacemaker neurons.

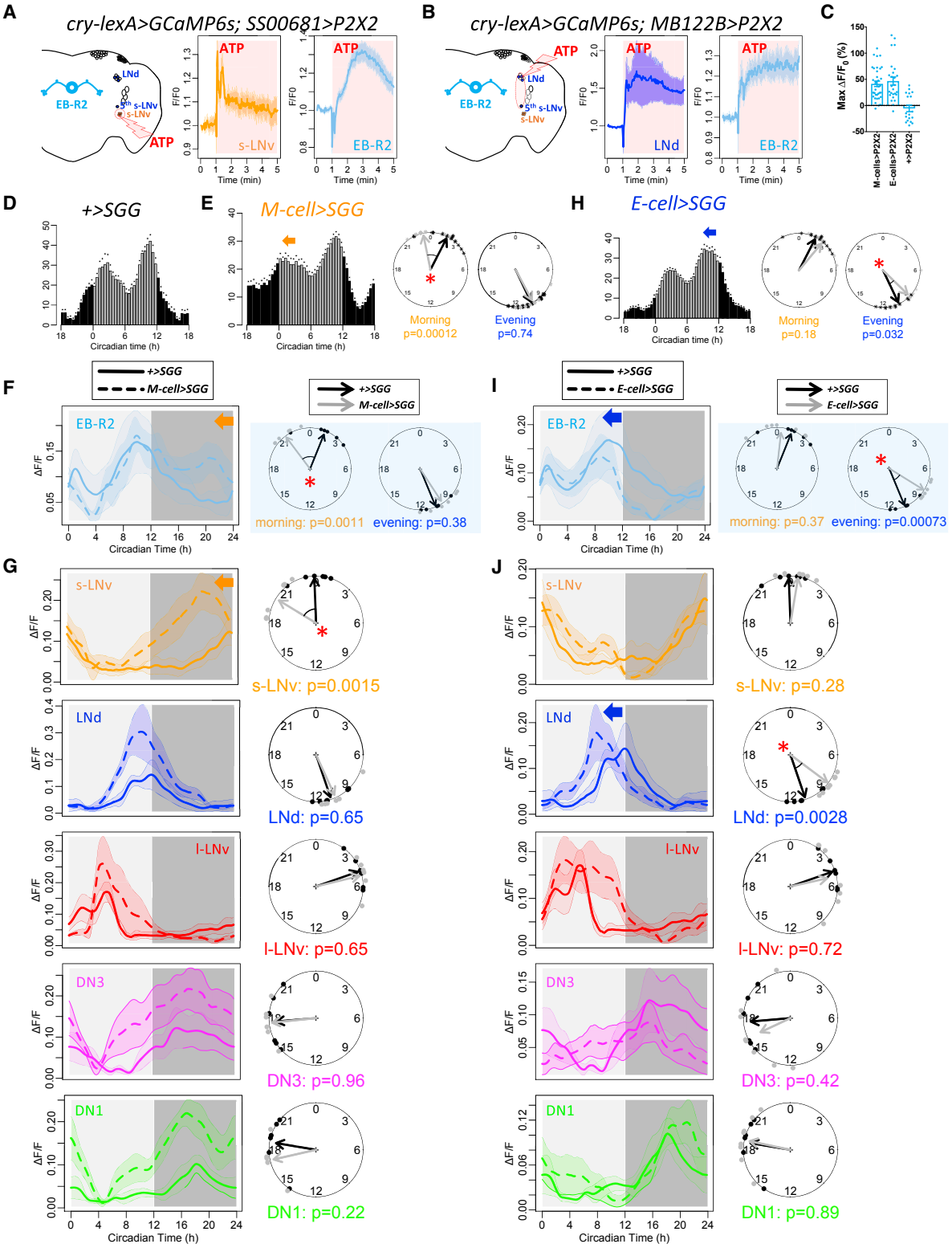

Figure 4. Daily Activity Phases of EB-RNs Are Dictated by M and E Cells

(A) Illustration and averaged response traces of M cells (s-LNv) and EB-R2 neurons to ATP application in flies with P2X2 expressed in M cells (n = 6 flies).

(B) Illustration and averaged response traces of E cells (three LNd and the 5th s-LNv neurons) and EB-R2 neurons to ATP application in flies with P2X2 expressed in E cells (n = 5 flies).

(legend continued on next page)

Distinct Circadian Neurons Dictate the Separate Phases of EB-RN Activity

In contrast to EB-RNs, all circadian pacemaker neurons showed single daily peaks of activity. This difference suggested that the daily two-peak activity pattern of EB-RNs could be generated by a combination of different circadian neuronal outputs. We considered the simplest model, that M cells could drive a morning activity peak in EB-RNs while E cells could independently drive EB-RN evening activity. To begin to test this possibility, we determined that EB-RNs responded to the selective activation of M cells (four s-LNv) by ATP application to brains expressing ATP-gated cation channel P2X2 (Lima and Miesenböck, 2005) in M cells (Figure 4A) first. A similar design to selectively activate E cells, the 5th s-LNv and three PDFR-positive LNd (Im and Taghert, 2010), produced correspondent EB-RN responses of comparable amplitude (Figures 4B, 4C, and S5D–S5F). These results support the proposition that both M cells and E cells have functional connections with EB-RNs.

Then, as a more stringent test, we asked whether selectively accelerating M or E oscillators would selectively influence the phase of either the morning and/or evening peak of EB-RN Ca^{2+} activity. Overexpressing shaggy (SSG) using *pdf-GAL4* (*M-cell* > *SGG*) to accelerate the molecular clocks selectively in morning oscillators advanced the morning peak of locomotor activity (*cf.* Stoleru et al., 2005) and the M-cell activity peak (Figures 4D–4F). In these flies, we found that only the morning peak of EB-RN Ca^{2+} activity was phase-advanced, while their evening Ca^{2+} peak phase was unaffected (Figure 4G). This result suggests that the morning peak of EB-RN activity is dictated predominantly by the phase of M cell activity. In parallel, we asked whether the evening peak of EB-RNs is dictated by the phase of E cell activity. Overexpressing SGG in E cells by using a split-GAL4 line, GMR_MB122B (Liang et al., 2017), selectively advanced the evening behavioral peak (Figure 4H) and the E-cell activity peak (Figure 4J). In these flies, we found that only the evening peak of EB-RN Ca^{2+} activity was phase-advanced and was by comparable amplitude to what we previously observed with M cell acceleration and M peak advance (Figure 4I). Taken together, these results reveal essential circuit links to demonstrate that M cells and E cells can independently dictate the two distinct phases of EB-RN pre-motor activity.

Dopaminergic Neurons Regulate EB-RNs

None of the ~150 circadian pacemaker neurons in *Drosophila* project directly to the EB (Helfrich-Förster, 2005). Therefore, we asked through which interneurons M cells and E cells might regulate daily neural activity in EB-RNs. A set of two dopaminergic (DA) neurons (named PPM3-EB) appeared as prominent candidates, as they innervate the EB. Further, they can initiate locomotor activity and promote ethanol-induced locomotor activity (Kong et al., 2010). First, we established that PPM3-EB neurons displayed a daily bimodal neural activity pattern *in vivo* spontaneously (Hartigans' dip test, $p < 0.0001$), similarly to that of the EB-RNs and consistent with their putative involvement in the daily profile of locomotor activity (Figure 5A). To study the precise relationship between activity in EB-RNs and that in PPM3-EBs, we employed dual-color Ca^{2+} imaging in single fly brains (Figure 5B). This method separated Ca^{2+} activity signals from these two anatomically overlapping neuron groups, by simultaneously recording a green signal in PPM3-EB (GCaMP6s) and a red signal in EB-RNs (jGECO1a, Dana et al., 2016). We found that the spontaneous Ca^{2+} activity patterns of EB-RNs were highly correlated with those of PPM3-EB, but poorly correlated with those of the l-LNv circadian neurons, which were also labeled by jGECO1a (Figures 5C–5F and S6C). This result suggests that PPM3-EB and EB-RNs are closely connected; they receive common inputs, and/or one receives synapses from the other. Next, we turned to anatomical analysis using the GRASP method (GFP reconstitution across synaptic partners; Feinberg et al., 2008). We expressed two complementary GFP fragments in PPM3-EB and EB-RNs respectively to demonstrate membrane appositions (potential synaptic connections) that normally exist between these two groups of neurons (Figures S6A and S6B). Furthermore, we asked whether the morning and evening activity peaks in PPM3-EB are independently dictated by M cells and E cells, respectively, as we showed for the bimodal activity patterns in the EB-RNs. Again, we overexpressed SSG using *pdf-GAL4* (PDF > SGG) to selectively advance the M-cell activity peak

(C) Maximum Ca^{2+} changes of EB-R2 after ATP application in experimental flies from (A) and (B) and from controls *(+/UAS-P2X2;cry-lexA>GCaMP6s*; n = 3 flies, also see Figures S5D–S5F).

(D) Average locomotor activity in DD1 of controls *(+>SGG;cry-lexA>GCaMP6s*; n = 16 flies).

(E) Left: average locomotor activity in DD1 of flies expressing SGG in PDF neurons (using *PDF-GAL4* (*M-cell)>SGG*, n = 16 flies). Right: phase comparisons of morning and evening activity between *+>SGG* and *M-cell > SGG*. Note that only the morning activity phase was significantly different (advanced, *$p < 0.05$, Watson-Williams test).

(F) Left: daily Ca^{2+} activity patterns during DD1 of EB-R2 neurons in *+>SGG;cry-lexA>GCaMP6s* flies (solid line, n = 6) and in *M-cell > SGG;cry-lexA>GCaMP6s* flies (dash line, n = 6). Note that the morning peak of EB-R2 was significantly advanced in *M-cell > SGG* (orange arrow). Right: phase comparisons of EB-R2 Ca^{2+} activity peaks between *+>SGG* (black points and arrow) and *M-cell > SGG* (gray points and arrow). The morning and evening activity peaks are displayed separately.

(G) Daily Ca^{2+} activity patterns and phase comparisons of circadian neurons in the same flies from (F): *+>SGG* flies (solid line, n = 6) and in *M-cell > SGG* flies (dash line, n = 6). Only peak phases of M cells (s-LNv) were significantly advanced in *M-cell > SGG* (*$p < 0.05$, Watson-Williams test).

(H) Left: average locomotor activity in DD1 of flies expressing SGG in E cells (using split-GAL4 line GMR_MB122B; *E-cell > SGG*, n = 16 flies). Right: phase comparisons of morning and evening locomotor activity between *+>SGG* and *E-cell > SGG*. Only evening activity phase was significantly different (advanced, *$p < 0.05$, Watson-Williams test).

(I) Daily Ca^{2+} activity patterns and phase comparisons of EB-R2 neurons between *+>SGG* flies (solid line, n = 6) and in *E-cell > SGG* flies (dash line, n = 8). The evening peak of EB-R2 were significantly advanced in *E-cell > SGG* (blue arrow).

(J) Daily Ca^{2+} activity patterns and phase comparisons of circadian neurons between *+>SGG* flies (solid line, n = 6) and in *E-cell > SGG* flies (dash line, n = 8). Only peak phases of E cells (LNd) were significantly advanced in *E-cell > SGG* (*$p < 0.05$, Watson-Williams test).

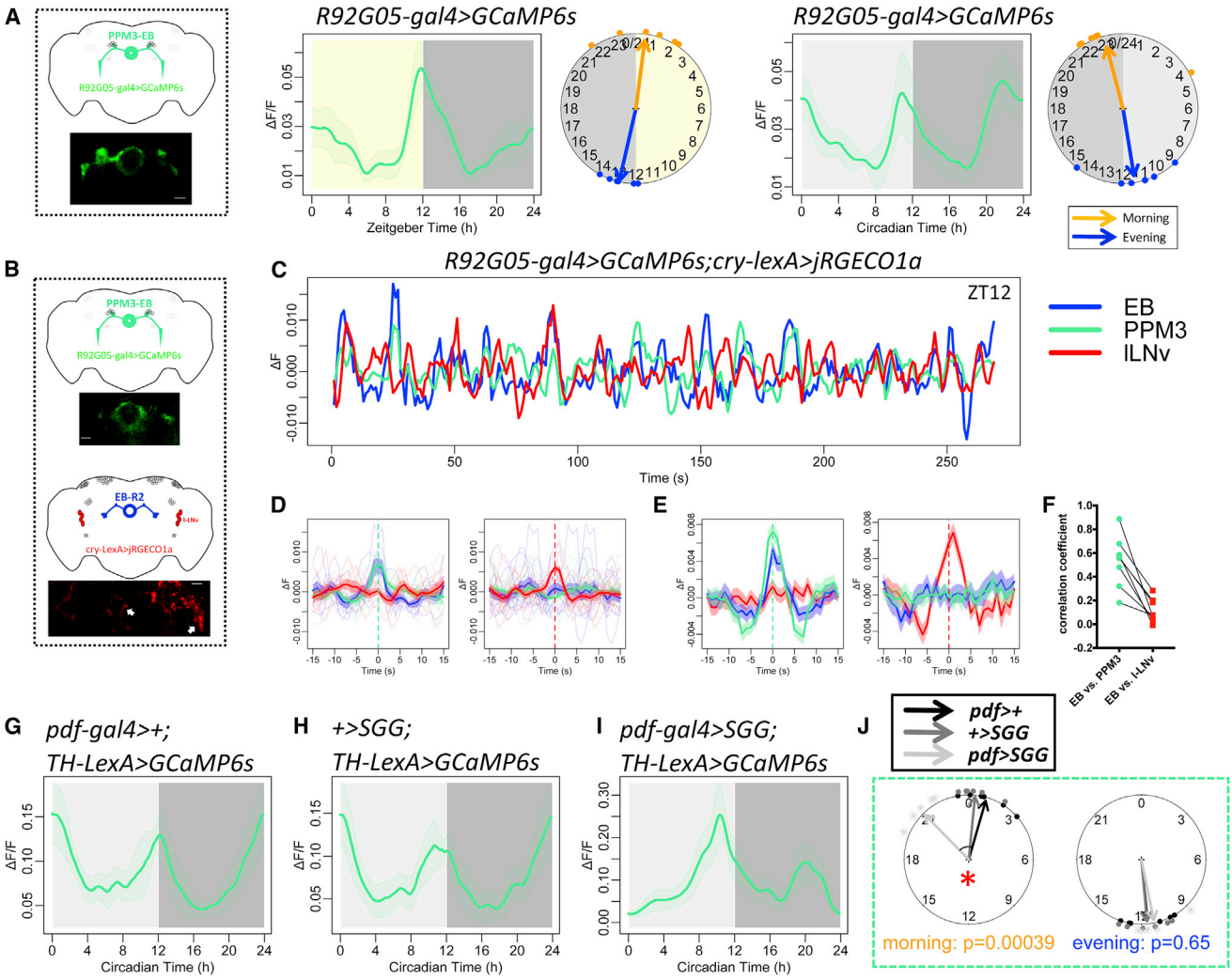

Figure 5. Daily Bimodal Pattern of PPM3-EB

(A) The position of the PPM3-EB neurons central complex in the fly brain (left). Daily bimodal Ca^{2+} activity patterns of PPM3-EB under LD (middle) and DD (right) (n = 6 flies each).

(B) Illustration of dual-color Ca^{2+} imaging: GCaMP6s in PPM3-EB and jRGECO1a in EB-R2 and in circadian neurons.

(C) Example traces of Ca^{2+} activity in EB-R2, PPM3-EB, and l-LNv neurons (sampling rate, 1 Hz).

(D) Average Ca^{2+} activity traces from (C) aligned by (left) PPM3-EB peak and (right) l-LNv peak.

(E) As in (D), average Ca^{2+} activity traces from all flies (n = 8 flies).

(F) Correlation of Ca^{2+} activity (Pearson's r) between EB and PPM3 is considerably stronger than that between EB and l-LNv (p = 0.0009, paired t test after Fisher's Z-transform).

(G-I) Daily Ca^{2+} activity patterns of PPM3 neurons during DD1 (G) in GAL-only control flies (n = 6 flies), (H) in UAS-only control flies (n = 6 flies), and (I) in *M-cell > SGG* flies (n = 5 flies).

(J) Phase comparisons of PPM3 neuron activity peaks for both morning (orange) and evening (blue) phases between controls and *M-cell > SGG* flies. The morning PPM3 peak was significantly advanced in *M-cell > SGG*, while the evening PPM3 peak was unaffected (Watson-Williams test).

(as in Figures 4D–4G). In these flies, we found that only the morning peak of PPM3-EB was phase advanced, while the evening peak phase was unaffected (Figures 5G–5J). This result suggested that the daily activity rhythm of PPM3-EB is driven by the same set of circadian neuron outputs as EB-RNs. Both PPM3-EB and EB-RNs responded to the bath application of PDF and to the pharmacogenetic activation of PDF neurons (Figures S6D and S6E). In response to the activation of PDF neurons, PPM3-EB responded more quickly than EB-RNs, which is consistent with PPM3-EBs occupying a physiological role "upstream" of EB-RNs. Together, these results support a model in which circadian pacemaker neurons indirectly activate as many as ~60 pairs of EB-RNs by first activating two pairs of dopaminergic neurons, the PPM3-EB.

We tested this model by blocking neurotransmission in PPM3-EB neurons, thereby asking whether their specific output is

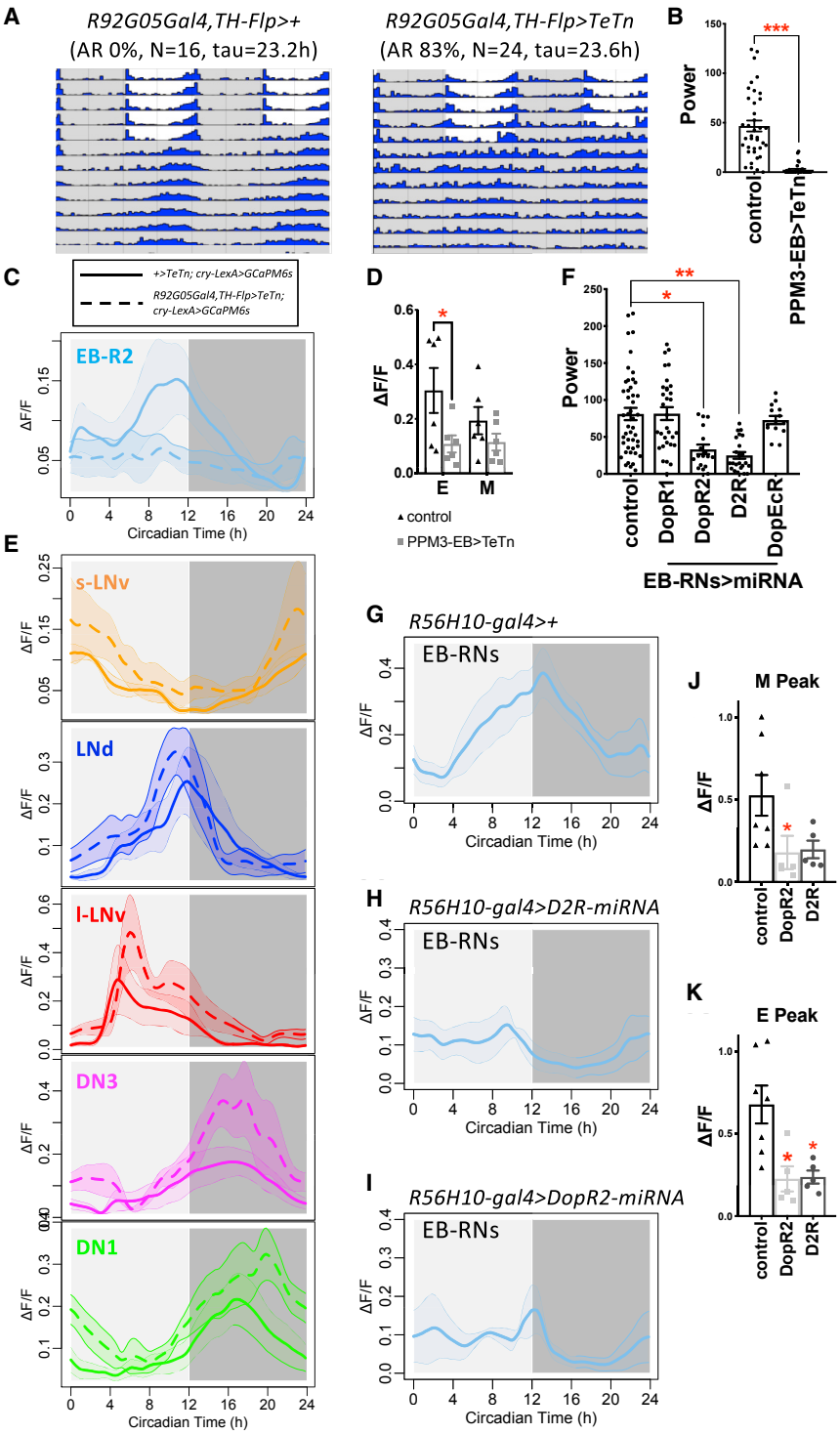

Figure 6. PPM3-EB and EB-RNs Constitute Downstream Elements of a Circadian Output Motor Circuit

(A) Group-averaged actograms of control flies (left) and one expressing tetanus toxin (TeTn) in PPM3-EB neurons to block neurotransmission (right).

(B) Average rhythm strength (power) of genotypes in (A) for 9 days under DD; asterisk denotes significant differences compared to control ($p < 0.0001$, Mann-Whitney test).

(C) Daily Ca^{2+} activity patterns of EB-R2 neurons during DD1 in control flies (solid line, n = 6) and ones with TeTn expressed in PPM3-EB neurons (*PPM3* > *TeTn*, dash line, n = 6).

(D) The amplitude of daily morning and evening Ca^{2+} peak in EB-R2 neurons in control and *PPM3* > *TeTn* flies. The amplitude difference in the evening peak was significantly different (*$p < 0.05$, Mann-Whitney test).

(E) Daily Ca^{2+} activity patterns of circadian neurons during DD1 in the same flies from (C): control flies (solid lines, n = 6) and *PPM3* > *TeTn* flies (dash line, n = 6).

(F) Average rhythm strength (power) of genotypes for 9 days under DD in which DA receptors are knocked down in EB-RNs using *R56H10-gal4*; asterisk denotes significant differences compared to control ($p < 0.05$, Kruskal-Wallis test followed by post hoc Dunn's tests). See more behavioral controls and statistics in Table S1.

(G–I) Daily Ca^{2+} activity patterns of EB-R neurons under DD1 in (G) WT (n = 8 flies), (H) flies with (H) *D2R*-knockdown, and (I) *DopR2*-knockdown in EB-R neurons (n = 5 and 5 flies).

(J and K) The amplitude of daily (J) morning and (K) evening Ca^{2+} peak in EB-R neurons was reduced in DA-receptor-knockdown flies (*$p < 0.05$, Mann-Whitney test).

necessary for proper locomotor rhythmicity. Using intersectional genetics (*GMR92G05-GAL4* and *TH-Flp*), we restricted the expression of TeTn (Sweeney et al., 1995) to the two pairs of PPM3-EB. The locomotor activity of these flies was largely arrhythmic under DD (Figures 6A and 6B). This behavioral deficit was comparable with and even more severe than that caused by blocking neurotransmission in the majority of EB-RNs (Figure 1B and Table S1). Importantly, while the molecular clocks and Ca^{2+} rhythms of circadian pacemaker neurons in these flies were intact (Figures 6E and S7), the daily bimodal neural activity pattern of EB-RNs was severely impaired (Figures 6C and 6D). Likewise, knocking down DA receptors DopR2 or D2R in the majority of EB-RNs also impaired rhythmicity in locomotor activity under DD (Figure 6F and Table S1). Significantly, these same DA-receptor knockdowns also suppressed the daily bimodal neural activity pattern of EB-RNs (Figures 6G–6K). Thus, we propose that dopaminergic input from PPM3-EB neurons forms a critical relay to regulate EB-generated locomotor activity, according to a multi-phasic circadian schedule.

The daily bimodal pattern of PPM3-EB suggested these dopaminergic neurons may release DA twice a day, once in the morning and again in the evening, to modulate the neural activity of

EB-RNs. To test this hypothesis, we measured the responses of EB-RNs to pharmacogenetic activation of PPM3-EB (Figures 7A and 7B) and to bath-application of dopamine (Figure 7C). Then, using $GRAB_{DA}$, a genetically encoded GPCR-activation-based-DA sensor (Sun et al., 2018), we asked when and how often during the 24-h day EB-RNs *in vivo* receive direct DA modulation. The $GRAB_{DA}$ sensor in the EB-R3 subgroup responded to bath application of DA with increased fluorescence (Figure 7D). Then, we recorded this signal *in vivo* for 24 h and observed a spontaneous, daily bimodal pattern of activation (Figure 7E), similar in pattern and phasing to the Ca^{2+} activity pattern of upstream dopaminergic PPM3-EB neurons and to the Ca^{2+} activity pattern of EB-RNs themselves. Collectively, these results suggested that the daily bimodal dopaminergic modulation from PPM-EB to EB-RNs relays two distinct circadian phase points from the pacemaker-neuron system. This dopaminergic modulation helps to generate daily bimodal patterns in the neural activity of EB-RNs and, thus, daily bimodal patterns in locomotor activity (Figure 7F).

DISCUSSION

Locomotor activity in *Drosophila* follows a daily bimodal rhythm that peaks around dawn and again around dusk. By measuring spontaneous neural activity *in vivo* across the 24-h day, we found that morning and evening circadian oscillators independently activate the pre-motor EB-RNs through the agency of PPM3-EB dopaminergic neurons. These findings provide the most detailed insights available in any model system by which pre-motor pathways are organized in response to phasic circadian pacemaker information. In addition, they indicate an unexpectedly obligate role for dopamine in the neural control of daily rhythmic locomotor activity. We based our conclusions on four lines of evidence. (1) Both PPM3-EB and EB-RNs display daily spontaneous bimodal neural activity patterns that precisely correlate with locomotor activity patterns peaking around dawn and dusk (Figures 1 and 5A). (2) Locomotor activity closely followed changes in EB-RN activity (Figure 2), while EB-RN activity was itself highly correlated with PPM3-EB activity (Figures 5B–5F). (3) Different phases of EB-RN circadian-rhythmic neural activity relied on independent inputs from circadian pacemakers, M cells and E cells, but did not rely at all on visual inputs or on the execution of locomotor behavior (Figures 3 and 4). (4) Both EB-RN activity rhythms and normal locomotor activity rhythms required PPM3-EB inputs (Figures 6A–6E); normal locomotor activity rhythms also required DA receptors on EB-RNs to receive inputs from PPM3-EB DA neurons (Figures 6F–6K). These data together support a model that features outputs from M cells and E cells sequentially and independently generating the two daily peaks of activity PPM3-EB DA neurons. These non-circadian PPM3-EB DA neurons in turn relay the phasic information to activate as many as ~60 pairs of EB-RNs, thereby generating the bimodal daily locomotor activity rhythm (Figure 7E).

Output Circuits Downstream of Circadian Pacemaker Neurons

Our findings constitute important steps in relating the activities of distinct circadian pacemaker neurons to downstream neural circuits. Selcho et al. (2017) recently described circadian pacemaker control of a peripheral clock in *Drosophila* to control steroid hormone secretion whose titers gate subsequent adult emergence (eclosion). In that output pathway, s-LNv activate the peptidergic PTTH neurons, which in turn activate the peripheral prothoracic gland. With respect to locomotor behavior, we found that M (s-LNv) cells and E (LNd) oscillators independently control the morning and evening neural activity phases in EB-RNs (Figure 4) and PPM3-EB (Figures 5G–5I). Two recent studies linked a different subset of circadian pacemakers (DN1s) to subgroups of EB-RNs, via subsets of neurons in the anterior optic tubercle (Lamaze et al., 2018; Guo et al., 2018). By manipulating activity in this pathway, both groups found effects on the balance between sleep and wake states. Thus, increasing lines of research indicate circadian- and sleep-regulating circuits impart timing information to govern behavior through the classic pre-motor centers of the central complex.

Based on previous limited screens, two other groups of identified peptidergic neurons were implicated as components of output circuits for locomotor activity rhythms in *Drosophila*. The two groups included ones that express the diuretic hormone 44 (DH44), an ortholog of mammalian CRF (Cavanaugh et al., 2014), and ones that express leucokinin (LK) (Cavey et al., 2016), whose receptor is related to the neurokinin receptors. DH44 neurons receive synaptic inputs from DN1 pacemaker neurons, and both DH44- and LK-neurons are required for proper locomotor activity rhythms under DD conditions. However, the connectivity by which these two groups of neuroendocrine neurons promote locomotor activity and phase-restrict it to morning or evening times is uncertain. The daily two-peak pattern of locomotor activity is different from the daily activity pattern of either LK neurons (which are more active in the evening; Cavey et al., 2016) or of DH44 neurons (which are more active in mid-day; Bai et al., 2018). Additionally, recent studies showed that LK neurons also mediate hunger signals to promote locomotor activity (Yurgel et al., 2019; Zandawala et al., 2018). These observations suggest that during daily locomotor activity peaks, flies might move to seek food, seek a mate, and/or respond to other internal drives, which might be coupled with circadian timing. Therefore, several parallel pathways may converge within the EB-RN pre-motor circuit to generate and shape daily behavioral patterns.

Dopaminergic Neurons under Circadian Regulation

Previous studies in flies and mice have shown that DA modulates circadian pacemaker circuits (Chang et al., 2006; Grippo et al., 2017; Hirsh et al., 2010; Klose et al., 2016; Landgraf et al., 2016; Shang et al., 2011, 2013). Our findings here show that circadian pacemaker neurons also regulate DA neuron activity. DA neurons responded to circadian neuron outputs (Figures 4A and 4B) and showed spontaneous circadian neural activity rhythms that were correlated with behavior (Figure 5). These findings correspond to earlier studies in mammals showing that circadian rhythms in DA neuron activity and in striatal DA content are dependent on master circadian pacemaker neurons in the SCN (Smith et al., 1992; Sleipness et al., 2007; Luo and Aston-Jones, 2009; Fifel et al., 2018). Deficits of DA neurons in patients and in animal models of Parkinson's disease caused

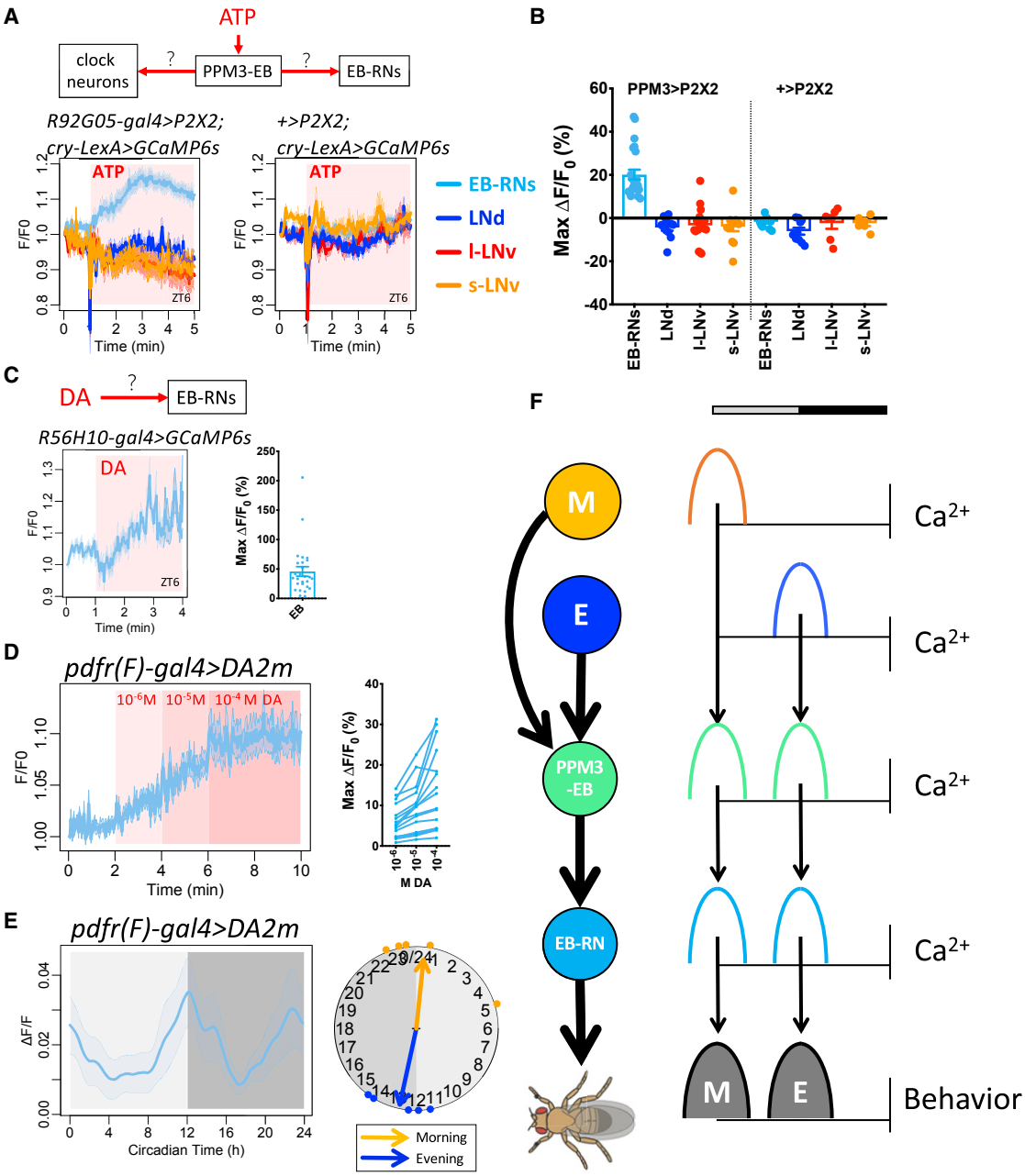

Figure 7. EB-RNs Receive Daily Bimodal Dopamine Inputs from PPM3-EB Neurons

(A) Average traces of EB-R2 neurons and circadian pacemaker neurons labeled by *cry-LexA,* responding to ATP (left) in flies with P2X2 expressing PPM3-EB DA neurons (n = 5 flies) and (right) *UAS-P2X2* only controls (n = 5 flies). Shaded area indicates duration of drug application. Error bars denote SEM.

(B) Maximum Ca^{2+} signal changes in individual cells within 4 min of ATP bath application.

(C) Left: average traces of EB-RNs responding to the bath-application of dopamine (10^{-4} M) at ZT6 (n = 4 flies). Right: maximum Ca^{2+} signal changes in individual cells within 3 min of DA bath application.

(D) Left: average traces of change from dopamine sensor $GRAB_{DA2m}$ in EB-R3 neurons responding to steps of DA bath application (10^{-6} M to 10^{-5} M to 10^{-4} M) at ZT6-8 (n = 4 flies). Right: maximum Ca^{2+} signal changes in individual cells within 2 min of different concentration of DA.

(E) The daily spontaneous bimodal pattern of signal from dopamine sensor $GRAB_{DA2m}$ in EB-R3 during DD1 (n = 5 flies).

(F) Model of the circadian output pathway for locomotor activity rhythms. Circadian pacemaker M cells and E cells independently activate EB-RN pre-motor circuits around dawn and dusk, respectively, through a relay by PPM3-EB dopaminergic neurons.

dysregulation of circadian locomotor activity patterns and of sleep (Videnovic and Golombek, 2017). Consistent with our model, a DA-deficient mouse model displays dampened and fragmented locomotor activity rhythms yet possesses normal SCN molecular clocks (Taylor et al., 2009; Kudo et al., 2011). It remains to be determined whether DA in mammals, as in *Drosophila*, represents the critical agent by which circadian outputs activate pre-motor centers to adaptively schedule locomotor activity.

The effects of DA to organize proper circadian control of locomotor behavior may be related to its well-documented effects in *Drosophila* to promote arousal, especially forms of arousal associated with changes in sleep and circadian rhythm states (Andretic et al., 2005; Birman, 2005; Kume et al., 2005; Lima and Miesenböck, 2005; Lebestky et al., 2009; Liu et al., 2012). A recent study suggests that PDF signals from circadian neurons promote wakefulness by suppressing daytime activity in the PPM3 DA neurons (Potdar and Sheeba, 2018). However, we favor an alternative model that is based on the results described above, including both manipulations of PPM3 physiology as well as measurements of normal PPM3 24-hr activity patterns *in vivo*. We propose PPM3-DA neurons promote wakefulness and locomotor activity in the morning following excitation by the M oscillators, perhaps directly by PDF.

How Can Circadian Timing Signals Modulate Activity in Central Complex to Promote Rhythmic Locomotor Activity?

Our results suggest that a major focus of circadian timing signals to regulate locomotor activity resides in the central complex, the decision-making circuit that dictates the balance between locomotion and rest. Within the central complex, EB neurons transform sensory inputs into goal-directed motor outputs (Sun et al., 2017; Shiozaki and Kazama, 2017). The final motor output is subject to many signals reflecting the internal state: for example, hunger signals transmitted through the leucokinin-expressing neurons promote locomotor activity (Yurgel et al., 2019; Zandawala et al., 2018). Here, we propose that the circadian system promotes locomotor activity in the dawn and dusk episodes by increasing the probability of the EB-RNs to favor activity over rest. A similar action on EB-RNs appears to underlie sleep promotion by dorsal fan-shaped body (dFSB) neurons (Donlea et al., 2018). dFSB neurons effectively suppress sensory-triggered movements by inhibiting EB-RNs via helicon cells and thereby instigate less activity and more rest. Thus, sleep and circadian signaling antagonistically converge on the EB-RN system to influence the level of motor output.

In addition to motor outputs, parts of EB circuits also signal the sleep drive; Liu et al. (2016) showed that a subgroup of EB-RNs, R2 (called R5 by Omoto et al., 2017), registers sleep debt and thereby constitutes an integral part of the sleep homeostat mechanism. How can this be reconciled with our finding that the EB-RNs (including R2s) exhibit neural activity in concert with locomotor behavior? We propose that, because the level of locomotor activity is directly encoded by EB-RN activity, a subgroup of them (R2s) incorporates the amount of locomotor activity along with duration of wakefulness to help generate sleep drive. Therefore, although they receive common circadian pacemaker and DA inputs, and although they exhibit common activation periods at dawn and at dusk, different subgroups of EB-RNs likely have specialized downstream functions in behavioral control.

Modulation of Locomotion in Vertebrates

The circuit features described by this work link pacemaker centers to premotor centers via specific DA interneurons. Could there be parallels across phylogeny? We note that a region between the vertebrate midbrain and hindbrain, the mesencephalic locomotor region (MLR), is implicated in the initiation and control of locomotion in numerous species, including lamprey, cat, rat, and monkey (reviewed by Ryczko and Duboc, 2013). Stimulation of the MLR elicits coordinated locomotion with varying speed and gait, depending on stimulus location (Caggiano et al., 2018). The MLR is heterogenous and includes the cuneiform and sub-cuneiform nuclei and the pedunculopontine nucleus. A traditional view held that DA modulated MLR activity indirectly via its projections to the basal ganglia (Ryczko and Duboc, 2013). In lampreys, however, the majority of DA neurons extend descending projections to the MLR that can modulate locomotor output (Ryczko et al., 2013). More recently, Ryczko et al. (2016) described direct DA inputs to MLR in the rat, from neurons that project to the striatum but also descend to the pedunculopontine nucleus. These authors propose that these direct DA inputs amplify subsequent MLR descending locomotor command. Also, Sharma et al. (2018) have described direct descending projections from A13 DA neurons of the mouse medial zona incerta to MLR nuclei. These authors speculate that A13 DA actions in the MLR may exhibit especially long time courses, because these neurons lack expression of the dopamine transporter. Together these observations support the hypothesis of a phylogenetically conserved DA-to-premotor pathway in vertebrates that amplifies signals to initiate and/or shape episodic locomotion. Thus, it may be worth investigating whether there exist functional connections between SCN circadian pacemaker outputs and these descending DA cell groups.

STAR★METHODS

Detailed methods are provided in the online version of this paper and include the following:

- KEY RESOURCES TABLE
- CONTACT FOR REAGENT AND RESOURCE SHARING
- EXPERIMENTAL MODEL AND SUBJECT DETAILS
  - Fly stocks
- METHOD DETAILS
  - Nomenclature
  - *In vivo* fly preparations
  - *In vivo* calcium imaging
  - Cameleon-based calcium imaging
  - *In vivo* dopamine imaging
  - Locomotor monitoring during imaging
  - Locomotor activity
  - Immunocytochemistry
  - Data reporting

- QUANTIFICATION AND STATISTICAL ANALYSIS
  - Imaging data analysis

SUPPLEMENTAL INFORMATION

Supplemental Information can be found online at https://doi.org/10.1016/j.neuron.2019.03.028.

ACKNOWLEDGMENTS

We thank Cody Greer for building the OCPI-2 microscope, the Holy and Taghert laboratories for advice, and the Washington University Center for Cellular Imaging (WUCCI) for technical support. Heather Dionne, Gerry Rubin, Aljoscha Nern, and Francois Rouyer kindly shared unpublished fly stocks and information. Orie Shafer, Michael Rosbash, the Bloomington Stock Center, and Janelia Research Center provided fly stocks and reagents. The work was supported by the Washington University McDonnell Center for Cellular and Molecular Neurobiology and by NIH grants, United States R01 NS068409 and R01 DP1 DA035081 (T.E.H.), R01 NS099332 and R01 GM127508 (P.H.T.), and R24 NS086741 (T.E.H. and P.H.T.); NIH Training Grant, United States T32HL110952 (M.C.W.H.) and R01NS079584 (M.N.W.); National Basic Research Program of China, China (973 Program; grant 2015CB856402 to Y.L.); the General Program of National Natural Science Foundation of China, China (project 31671118 to Y.L.); NIH BRAIN Initiative grant, United States U01NS103558 (Y.L.); and a Peking University Postdoctoral Fellowship, China (Y.Z.).

AUTHOR CONTRIBUTIONS

X.L., M.N.W., T.E.H., and P.H.T. conceived the experiments; X.L. performed and analyzed all experiments; M.C.W.H. generated and characterized the dopamine-related transgenic fly lines; Y.Z. and Y.L. generated the dopamine sensor $GRAB_{DA2m}$ fly line; and X.L., M.C.W.H., M.N.W., T.E.H., and P.H.T. wrote the manuscript.

DECLARATION OF INTERESTS

The authors declare no competing interests. T.E.H. has a patent on OCPI microscopy.

Received: November 16, 2018
Revised: February 6, 2019
Accepted: March 19, 2019
Published: April 10, 2019

REFERENCES

Andretic, R., van Swinderen, B., and Greenspan, R.J. (2005). Dopaminergic modulation of arousal in Drosophila. Curr. Biol. *15*, 1165–1175.

Bai, L., Lee, Y., Hsu, C.T., Williams, J.A., Cavanaugh, D., Zheng, X., Stein, C., Haynes, P., Wang, H., Gutmann, D.H., and Sehgal, A. (2018). A conserved circadian function for the *Neurofibromatosis 1* gene. Cell Rep. *22*, 3416–3426.

Berry, J.A., Cervantes-Sandoval, I., Chakraborty, M., and Davis, R.L. (2015). Sleep facilitates memory by blocking dopamine neuron-mediated forgetting. Cell *161*, 1656–1667.

Birman, S. (2005). Arousal mechanisms: speedy flies don't sleep at night. Curr. Biol. *15*, R511–R513.

Blau, J., and Young, M.W. (1999). Cycling vrille expression is required for a functional Drosophila clock. Cell *99*, 661–671.

Caggiano, V., Leiras, R., Goñi-Erro, H., Masini, D., Bellardita, C., Bouvier, J., Caldeira, V., Fisone, G., and Kiehn, O. (2018). Midbrain circuits that set locomotor speed and gait selection. Nature *553*, 455–460.

Cavanaugh, D.J.J., Geratowski, J.D.D., Wooltorton, J.R.A., Spaethling, J.M.M., Hector, C.E.E., Zheng, X., Johnson, E.C.C., Eberwine, J.H.H., and Sehgal, A. (2014). Identification of a circadian output circuit for rest:activity rhythms in Drosophila. Cell *157*, 689–701.

Cavey, M., Collins, B., Bertet, C., and Blau, J. (2016). Circadian rhythms in neuronal activity propagate through output circuits. Nat. Neurosci. *19*, 587–595.

Chang, H.Y., Grygoruk, A., Brooks, E.S., Ackerson, L.C., Maidment, N.T., Bainton, R.J., and Krantz, D.E. (2006). Overexpression of the Drosophila vesicular monoamine transporter increases motor activity and courtship but decreases the behavioral response to cocaine. Mol. Psychiatry *11*, 99–113.

Chen, T.W., Wardill, T.J., Sun, Y., Pulver, S.R., Renninger, S.L., Baohan, A., Schreiter, E.R., Kerr, R.A., Orger, M.B., Jayaraman, V., et al. (2013). Ultrasensitive fluorescent proteins for imaging neuronal activity. Nature *499*, 295–300.

Dana, H., Mohar, B., Sun, Y., Narayan, S., Gordus, A., Hasseman, J.P., Tsegaye, G., Holt, G.T., Hu, A., Walpita, D., et al. (2016). Sensitive red protein calcium indicators for imaging neural activity. eLife *5*, e12727.

de la Iglesia, H.O., Meyer, J., and Schwartz, W.J. (2003). Lateralization of circadian pacemaker output: Activation of left- and right-sided luteinizing hormone-releasing hormone neurons involves a neural rather than a humoral pathway. J. Neurosci. *23*, 7412–7414.

Donlea, J.M., Pimentel, D., Talbot, C.B., Kempf, A., Omoto, J.J., Hartenstein, V., and Miesenböck, G. (2018). Recurrent circuitry for balancing sleep need and sleep. Neuron *97*, 378–389.e4.

Feinberg, E.H., Vanhoven, M.K., Bendesky, A., Wang, G., Fetter, R.D., Shen, K., and Bargmann, C.I. (2008). GFP Reconstitution Across Synaptic Partners (GRASP) defines cell contacts and synapses in living nervous systems. Neuron *57*, 353–363.

Fifel, K., Meijer, J.H., and Deboer, T. (2018). Circadian and Homeostatic Modulation of Multi-Unit Activity in Midbrain Dopaminergic Structures. Sci. Rep. *8*, 7765.

Froy, O., Gotter, A.L., Casselman, A.L., and Reppert, S.M. (2003). Illuminating the circadian clock in monarch butterfly migration. Science *300*, 1303–1305.

Greer, C.J., and Holy, T.E. (2018). Fast objective coupled planar illumination microscopy. bioRxiv. https://doi.org/10.1101/501890.

Grima, B., Chélot, E., Xia, R., and Rouyer, F. (2004). Morning and evening peaks of activity rely on different clock neurons of the *Drosophila* brain. Nature *431*, 869–873.

Grippo, R.M., Purohit, A.M., Zhang, Q., Zweifel, L.S., and Güler, A.D. (2017). Direct midbrain dopamine input to the suprachiasmatic nucleus accelerates circadian entrainment. Curr. Biol. *27*, 2465–2475.e3.

Guo, F., Yu, J., Jung, H.J., Abruzzi, K.C., Luo, W., Griffith, L.C., and Rosbash, M. (2016). Circadian neuron feedback controls the Drosophila sleep–activity profile. Nature *536*, 292–297.

Guo, F., Holla, M., Díaz, M.M., and Rosbash, M. (2018). A circadian output circuit controls sleep-wake arousal in Drosophila. Neuron *100*, 624–635.e4.

Hartigan, J.A., and Hartigan, P.M. (1985). The dip test of unimodality. J. Am. Stat. Assoc. *86*, 738–746.

Heinze, S., and Reppert, S.M. (2011). Sun compass integration of skylight cues in migratory monarch butterflies. Neuron *69*, 345–358.

Helfrich-Förster, C. (2005). Neurobiology of the fruit fly's circadian clock. Genes Brain Behav. *4*, 65–76.

Hirsh, J., Riemensperger, T., Coulom, H., Iché, M., Coupar, J., and Birman, S. (2010). Roles of dopamine in circadian rhythmicity and extreme light sensitivity of circadian entrainment. Curr. Biol. *20*, 209–214.

Holekamp, T.F., Turaga, D., and Holy, T.E. (2008). Fast three-dimensional fluorescence imaging of activity in neural populations by objective-coupled planar illumination microscopy. Neuron *57*, 661–672.

Hyun, S., Lee, Y., Hong, S.-T., Bang, S., Paik, D., Kang, J., Shin, J., Lee, J., Jeon, K., Hwang, S., et al. (2005). *Drosophila* GPCR Han is a receptor for the circadian clock neuropeptide PDF. Neuron *48*, 267–278.

Im, S.H., and Taghert, P.H. (2010). PDF receptor expression reveals direct interactions between circadian oscillators in Drosophila. J. Comp. Neurol. *518*, 1925–1945.

Kalsbeek, A., Palm, I.F., La Fleur, S.E., Scheer, F.A., Perreau-Lenz, S., Ruiter, M., Kreier, F., Cailotto, C., and Buijs, R.M. (2006). SCN outputs and the hypothalamic balance of life. J. Biol. Rhythms *21*, 458–469.

Kaneko, M., and Hall, J.C. (2000). Neuroanatomy of cells expressing clock genes in *Drosophila*: transgenic manipulation of the period and timeless genes to mark the perikarya of circadian pacemaker neurons and their projections. J. Comp. Neurol. *422*, 66–94.

Klose, M., Duvall, L., Li, W., Liang, X., Ren, C., Steinbach, J.H.H., and Taghert, P.H. (2016). Functional PDF signaling in the Drosophila circadian neural circuit is gated by Ral A-Dependent modulation. Neuron *90*, 781–794.

Kong, E.C., Woo, K., Li, H., Lebestky, T., Mayer, N., Sniffen, M.R., Heberlein, U., Bainton, R.J., Hirsh, J., and Wolf, F.W. (2010). A pair of dopamine neurons target the D1-like dopamine receptor *DopR* in the central complex to promote ethanol-stimulated locomotion in Drosophila. PLoS ONE *5*, e9954.

Konopka, R.J., and Benzer, S. (1971). Clock mutants of Drosophila melanogaster. Proc. Natl. Acad. Sci. USA *68*, 2112–2116.

Kudo, T., Loh, D.H., Truong, D., Wu, Y., and Colwell, C.S. (2011). Circadian dysfunction in a mouse model of Parkinson's disease. Exp. Neurol. *232*, 66–75.

Kume, K., Kume, S., Park, S.K., Hirsh, J., and Jackson, F.R. (2005). Dopamine is a regulator of arousal in the fruit fly. J. Neurosci. *25*, 7377–7384.

Lamaze, A., Krätschmer, P., Chen, K.F., Lowe, S., and Jepson, J.E.C. (2018). A wake-promoting circadian output circuit in Drosophila. Curr. Biol. *28*, 3098–3105.e3.

Landgraf, D., Joiner, W.J., McCarthy, M.J., Kiessling, S., Barandas, R., Young, J.W., Cermakian, N., and Welsh, D.K. (2016). The mood stabilizer valproic acid opposes the effects of dopamine on circadian rhythms. Neuropharmacology *107*, 262–270.

Lebestky, T., Chang, J.S., Dankert, H., Zelnik, L., Kim, Y.C., Han, K.A., Wolf, F.W., Perona, P., and Anderson, D.J. (2009). Two different forms of arousal in *Drosophila* are oppositely regulated by the dopamine D1 receptor ortholog DopR via distinct neural circuits. Neuron *64*, 522–536.

Lehman, M.N., Silver, R., Gladstone, W.R., Kahn, R.M., Gibson, M., and Bittman, E.L. (1987). Circadian rhythmicity restored by neural transplant. Immunocytochemical characterization of the graft and its integration with the host brain. J. Neurosci. *7*, 1626–1638.

Levine, J.D., Funes, P., Dowse, H.B., and Hall, J.C. (2002). Signal analysis of behavioral and molecular cycles. BMC Neurosci. *3*, 1–25.

Liang, X., Holy, T.E., and Taghert, P.H. (2016). Synchronous Drosophila circadian pacemakers display nonsynchronous Ca^{2+} rhythms in vivo. Science *351*, 976–981.

Liang, X., Holy, T.E., and Taghert, P.H. (2017). A series of suppressive signals within the *Drosophila* circadian neural circuit generates sequential daily outputs. Neuron *94*, 1173–1189.e4.

Lima, S.Q., and Miesenböck, G. (2005). Remote control of behavior through genetically targeted photostimulation of neurons. Cell *121*, 141–152.

Liu, Q., Liu, S., Kodama, L., Driscoll, M.R., and Wu, M.N. (2012). Two dopaminergic neurons signal to the dorsal fan-shaped body to promote wakefulness in Drosophila. Curr. Biol. *22*, 2114–2123.

Liu, S., Liu, Q., Tabuchi, M., and Wu, M.N. (2016). Sleep drive is encoded by neural plastic changes in a dedicated circuit. Cell *165*, 1347–1360.

Liu, Q., Tabuchi, M., Liu, S., Kodama, L., Horiuchi, W., Daniels, J., Chiu, L., Baldoni, D., and Wu, M.N. (2017). Branch-specific plasticity of a bifunctional dopamine circuit encodes protein hunger. Science *356*, 534–539.

Luo, A.H., and Aston-Jones, G. (2009). Circuit projection from suprachiasmatic nucleus to ventral tegmental area: a novel circadian output pathway. Eur. J. Neurosci. *29*, 748–760.

Macpherson, L.J., Zaharieva, E.E., Kearney, P.J., Alpert, M.H., Lin, T.Y., Turan, Z., Lee, C.H., and Gallio, M. (2015). Dynamic labelling of neural connections in multiple colours by trans-synaptic fluorescence complementation. Nat. Commun. *6*, 10024.

Martín-Peña, A., Acebes, A., Rodríguez, J.R., Chevalier, V., Casas-Tinto, S., Triphan, T., Strauss, R., and Ferrús, A. (2014). Cell types and coincident synapses in the ellipsoid body of *Drosophila*. Eur. J. Neurosci. *39*, 1586–1601.

Martinek, S., Inonog, S., Manoukian, A.S., and Young, M.W. (2001). A role for the segment polarity gene *shaggy/GSK-3* in the Drosophila circadian clock. Cell *105*, 769–779.

Miyawaki, A., Griesbeck, O., Heim, R., and Tsien, R.Y. (1999). Dynamic and quantitative Ca^{2+} measurements using improved cameleons. Proc. Natl. Acad. Sci. USA *96*, 2135–2140.

Moore, R.Y., and Klein, D.C. (1974). Visual pathways and the central neural control of a circadian rhythm in pineal serotonin N-acetyltransferase activity. Brain Res. *71*, 17–33.

Neuser, K., Triphan, T., Mronz, M., Poeck, B., and Strauss, R. (2008). Analysis of a spatial orientation memory in Drosophila. Nature *453*, 1244–1247.

Nitabach, M.N., and Taghert, P.H. (2008). Organization of the Drosophila circadian control circuit. Curr. Biol. *18*, R84–R93.

Ofstad, T.A., Zuker, C.S., and Reiser, M.B. (2011). Visual place learning in *Drosophila* melanogaster. Nature *474*, 204–207.

Omoto, J.J., Keleş, M.F., Nguyen, B.M., Bolanos, C., Lovick, J.K., Frye, M.A., and Hartenstein, V. (2017). Visual Input to the Drosophila Central Complex by Developmentally and Functionally Distinct Neuronal Populations. Curr. Biol. *27*, 1098–1110.

Ostroy, S.E., and Pak, W.L. (1974). Protein and electroretinogram changes in the alleles of the norp AP12 Drosophila phototransduction mutant. Biochim. Biophys. Acta *368*, 259–268.

Pfeiffer, K., and Homberg, U. (2014). Organization and functional roles of the central complex in the insect brain. Annu. Rev. Entomol. *59*, 165–184.

Potdar, S., and Sheeba, V. (2018). Wakefulness is promoted during day time by PDFR signalling to dopaminergic neurons in Drosophila melanogaster. eNeuro *5*, ENEURO.0129-18.2018.

Ralph, M.R., Foster, R.G., Davis, F.C., and Menaker, M. (1990). Transplanted suprachiasmatic nucleus determines circadian period. Science *247*, 975–978.

Renn, S.C.P., Armstrong, J.D., Yang, M., Wang, Z., An, X., Kaiser, K., and Taghert, P.H. (1999a). Genetic analysis of the *Drosophila* ellipsoid body neuropil: organization and development of the central complex. J. Neurobiol. *41*, 189–207.

Renn, S.C., Park, J.H., Rosbash, M., Hall, J.C., and Taghert, P.H. (1999b). A *pdf* neuropeptide gene mutation and ablation of PDF neurons each cause severe abnormalities of behavioral circadian rhythms in Drosophila. Cell *99*, 791–802.

Robie, A.A., Hirokawa, J., Edwards, A.W., Umayam, L.A., Lee, A., Phillips, M.L., Card, G.M., Korff, W., Rubin, G.M., Simpson, J.H., et al. (2017). Mapping the neural substrates of behavior. Cell *170*, 393–406.e28.

Ryczko, D., and Dubuc, R. (2013). The multifunctional mesencephalic locomotor region. Curr. Pharm. Des. *19*, 4448–4470.

Ryczko, D., Grätsch, S., Auclair, F., Dubé, C., Bergeron, S., Alpert, M.H., Cone, J.J., Roitman, M.F., Alford, S., and Dubuc, R. (2013). Forebrain dopamine neurons project down to a brainstem region controlling locomotion. Proc. Natl. Acad. Sci. USA *110*, E3235–E3242.

Ryczko, D., Cone, J.J., Alpert, M.H., Goetz, L., Auclair, F., Dubé, C., Parent, M., Roitman, M.F., Alford, S., and Dubuc, R. (2016). A descending dopamine pathway conserved from basal vertebrates to mammals. Proc. Natl. Acad. Sci. USA *113*, E2440–E2449.

Schindelin, J., Arganda-Carreras, I., Frise, E., Kaynig, V., Longair, M., Pietzsch, T., Preibisch, S., Rueden, C., Saalfeld, S., Schmid, B., et al. (2012). Fiji: an open-source platform for biological-image analysis. Nat. Methods *9*, 676–682.

Seelig, J.D., and Jayaraman, V. (2013). Feature detection and orientation tuning in the Drosophila central complex. Nature *503*, 262–266.

Selcho, M., Millán, C., Palacios-Muñoz, A., Ruf, F., Ubillo, L., Chen, J., Bergmann, G., Ito, C., Silva, V., Wegener, C., and Ewer, J. (2017). Central and peripheral clocks are coupled by a neuropeptide pathway in Drosophila. Nat. Commun. *8*, 15563.

Shang, Y., Griffith, L.C., and Rosbash, M. (2008). Light-arousal and circadian photoreception circuits intersect at the large PDF cells of the Drosophila brain. Proc. Natl. Acad. Sci. U.S.A. *105*, 19587–19594.

Shang, Y., Haynes, P., Pírez, N., Harrington, K.I., Guo, F., Pollack, J., Hong, P., Griffith, L.C., and Rosbash, M. (2011). Imaging analysis of clock neurons reveals light buffers the wake-promoting effect of dopamine. Nat. Neurosci. *14*, 889–895.

Shang, Y., Donelson, N.C., Vecsey, C.G., Guo, F., Rosbash, M., and Griffith, L.C. (2013). Short neuropeptide F is a sleep-promoting inhibitory modulator. Neuron *80*, 171–183.

Sharma, S., Kim, L.H., Mayr, K.A., Elliott, D.A., and Whelan, P.J. (2018). Parallel descending dopaminergic connectivity of A13 cells to the brainstem locomotor centers. Sci. Rep. *8*, 7972.

Shiozaki, H.M., and Kazama, H. (2017). Parallel encoding of recent visual experience and self-motion during navigation in Drosophila. Nat. Neurosci. *20*, 1395–1403.

Silverman, B.W. (1981). Using kernel density estimates to investigate multimodality. J. R. Stat. Soc. B. *43*, 97–99.

Sleipness, E.P., Sorg, B.A., and Jansen, H.T. (2007). Diurnal differences in dopamine transporter and tyrosine hydroxylase levels in rat brain: dependence on the suprachiasmatic nucleus. Brain Res. *1129*, 34–42.

Smith, A.D., Olson, R.J., and Justice, J.B., Jr. (1992). Quantitative microdialysis of dopamine in the striatum: effect of circadian variation. J. Neurosci. Methods *44*, 33–41.

Stanewsky, R., Jamison, C.F., Plautz, J.D., Kay, S.A., and Hall, J.C. (1997). Multiple circadian-regulated elements contribute to cycling period gene expression in Drosophila. EMBO J. *16*, 5006–5018.

Stoleru, D., Peng, Y., Agosto, J., and Rosbash, M. (2004). Coupled oscillators control morning and evening locomotor behaviour of Drosophila. Nature *431*, 862–868.

Stoleru, D., Peng, Y., Nawathean, P., and Rosbash, M. (2005). A resetting signal between Drosophila pacemakers synchronizes morning and evening activity. Nature *438*, 238–242.

Strauss, R., and Heisenberg, M. (1993). A higher control center of locomotor behavior in the *Drosophila* brain. J. Neurosci. *13*, 1852–1861.

Sun, Y., Nern, A., Franconville, R., Dana, H., Schreiter, E.R., Looger, L.L., Svoboda, K., Kim, D.S., Hermundstad, A.M., and Jayaraman, V. (2017). Neural signatures of dynamic stimulus selection in Drosophila. Nat. Neurosci. *20*, 1104–1113.

Sun, F., Zeng, J., Jing, M., Zhou, J., Feng, J., Owen, S.F., Luo, Y., Li, F., Wang, H., Yamaguchi, T., et al. (2018). A genetically encoded fluorescent sensor enables rapid and specific detection of dopamine in flies, fish, and mice. Cell *174*, 481–496.e19.

Sweeney, S.T., Broadie, K., Keane, J., Niemann, H., and O'Kane, C.J. (1995). Targeted expression of tetanus toxin light chain in Drosophila specifically eliminates synaptic transmission and causes behavioral defects. Neuron *14*, 341–351.

Taylor, T.N., Caudle, W.M., Shepherd, K.R., Noorian, A., Jackson, C.R., Iuvone, P.M., Weinshenker, D., Greene, J.G., and Miller, G.W. (2009). Nonmotor symptoms of Parkinson's disease revealed in an animal model with reduced monoamine storage capacity. J. Neurosci. *29*, 8103–8113.

VanderLeest, H.T., Houben, T., Michel, S., Deboer, T., Albus, H., Vansteensel, M.J., Block, G.D., and Meijer, J.H. (2007). Seasonal encoding by the circadian pacemaker of the SCN. Curr. Biol. *17*, 468–473.

Videnovic, A., and Golombek, D. (2017). Circadian dysregulation in Parkinson's disease. Neurobiol Sleep Circadian Rhythms *2*, 53–58.

Xie, T., Ho, M.C.W., Liu, Q., Horiuchi, W., Lin, C.-C.C., Task, D., Luan, H., White, B.H., Potter, C.J., and Wu, M.N. (2018). A genetic toolkit for dissecting dopamine circuit function in Drosophila. Cell Rep. *23*, 652–665.

Yao, Z., and Shafer, O.T. (2014). The Drosophila circadian clock is a variably coupled network of multiple peptidergic units. Science *343*, 1516–1520.

Yao, Z., Macara, A.M., Lelito, K.R., Minosyan, T.Y., and Shafer, O.T. (2012). Analysis of functional neuronal connectivity in the Drosophila brain. J. Neurophysiol. *108*, 684–696.

Yoshii, T., Funada, Y., Ibuki-Ishibashi, T., Matsumoto, A., Tanimura, T., and Tomioka, K. (2004). Drosophila cry^b mutation reveals two circadian clocks that drive locomotor rhythm and have different responsiveness to light. J. Insect Physiol. *50*, 479–488.

Yurgel, M.E., Kakad, P., Zandawala, M., Nässel, D.R., Godenschwege, T.A., and Keene, A.C. (2019). A single pair of leucokinin neurons are modulated by feeding state and regulate sleep–metabolism interactions. PLoS Biol. *17*, e2006409.

Zandawala, M., Yurgel, M.E., Texada, M.J., Liao, S., Rewitz, K.F., Keene, A.C., and Nässel, D.R. (2018). Modulation of Drosophila post-feeding physiology and behavior by the neuropeptide leucokinin. PLoS Genet. *14*, e1007767.

Zhang, Y., Liu, Y., Bilodeau-Wentworth, D., Hardin, P.E., and Emery, P. (2010). Light and temperature control the contribution of specific DN1 neurons to Drosophila circadian behavior. Curr. Biol. *20*, 600–605.

STAR★METHODS

KEY RESOURCES TABLE

REAGENT or RESOURCE	SOURCE	IDENTIFIER
Chemicals, Peptides, and Recombinant Proteins		
Adenosine 5′-triphosphate	Sigma	A5394
Dopamine hydrochloride	Sigma	H8502
Drosophila pigment dispersing factor (PDF)	Neo-MPS	N/A
Experimental Models: Organisms/Strains		
Drosophila: tim(UAS)-GAL4	Blau and Young, 1999	N/A
Drosophila: pdfr(B)-GAL4	Taghert Lab, (Im and Taghert, 2010)	N/A
Drosophila: pdfr(F)-GAL4	Taghert Lab, (Im and Taghert, 2010)	N/A
Drosophila: pdf-LexA	Shang et al., 2008	N/A
Drosophila: LexAop-nSyb-spGFP1-10, UAS-CD4-spGFP11	Bloomington (Macpherson et al., 2015)	RRID: BDSC_64315
Drosophila:20XUAS-IVS-GCaMP6s(attP40)	Bloomington (Chen et al., 2013)	RRID: BDSC_42746
Drosophila:13XLexAop2-IVS-GCaMP6s-p10(su(Hw)attP1)	Bloomington (Chen et al., 2013)	RRID: BDSC_44274
Drosophila: LexAop-jGECO1a	Bloomington (Dana et al., 2016)	RRID: BDSC_63794
Drosophila: UAS-(FRT.stop)-TeTn	Bloomington	RRID: BDSC_67690
Drosophila: UAS-SGG	Bloomington (Martinek et al., 2001)	RRID: BDSC_5435
Drosophila: UAS-GRAB$_{DA2m}$	Yulong Li (Sun et al., 2018)	N/A
Drosophila: UAS-P2X2	Orie Shafer (Yao et al., 2012)	N/A
Drosophila: UAS-cameleon2.1	Bloomington (Miyawaki et al., 1999)	RRID: BDSC_6901
Drosophila: LexAop-P2X2	Orie Shafer (Yao et al., 2012)	N/A
Drosophila: cry-LexA::GAD	F. Rouyer (CNRS Gyf, Paris) (Liang et al., 2017)	N/A
Drosophila: TH-LexA	Berry et al., 2015	N/A
Drosophila: GMR_SS00681	Gifts from Drs. Dionne, Nern and Rubin (Janelia Research Center, VA) (Liang et al., 2017)	N/A
Drosophila: GMR_MB122B	Gifts from Drs. Dionne, Nern and Rubin (Janelia Research Center, VA) (Liang et al., 2017)	N/A
Drosophila: GMR_SS002769	Janelia Research Center (Robie et al., 2017)	N/A
Drosophila: GMR56H10-GAL4	Bloomington (Sun et al., 2017)	RRID: BDSC_61644
Drosophila: GMR96F08-GAL4	Bloomington (Liu et al., 2016)	RRID: BDSC_39499
Drosophila: GMR92G05-GAL4	Bloomington (Xie et al., 2018)	RRID: BDSC_48416
Drosophila: GMR19C08-LexA	Bloomington	RRID: BDSC_53543
Drosophila: norpA^{P24}	Bloomington (Ostroy and Pak, 1974)	RRID: BDSC_9048
Drosophila: per^{01}	Konopka and Benzer, 1971	N/A
Drosophila: pdfr^{han5403}	Hyun et al., 2005	N/A
Drosophila: UAS-DopR1-miRNA	Wu Lab (Liu et al., 2017)	N/A
Drosophila: UAS-DopR2-miRNA	Wu Lab (Liu et al., 2017)	N/A
Drosophila: UAS-D2R-miRNA	Wu Lab (Xie et al., 2018)	N/A
Drosophila: UAS-DopEcR-miRNA	Wu Lab (Xie et al., 2018)	N/A
Drosophila: TH-Flp	Wu Lab (Xie et al., 2018)	N/A
Software and Algorithms		
R	http://www.R-project.org/	Version: 3.3.3
Julia	https://julialang.org/	Version: 0.6
Prism 7	GraphPad	https://www.graphpad.com/
Fiji	(Schindelin et al., 2012)	https://fiji.sc/
Imagine	(Holekamp et al., 2008)	http://holylab.wustl.edu/

CONTACT FOR REAGENT AND RESOURCE SHARING

Further information and requests for reagents may be directed to and will be fulfilled by the Lead Contact, Paul H. Taghert (taghertp@wustl.edu).

EXPERIMENTAL MODEL AND SUBJECT DETAILS

Fly stocks

Flies were reared on standard cornmeal/agar food at room temperature. Before imaging experiments, flies were entrained under 12 h light: 12 h dark (LD) cycles at 25°C for at least 3 days. Male flies, 3-10 days old, were selected for imaging. The following fly lines were previously described: *tim(UAS)-GAL4* (Blau and Young, 1999), *pdfr(F)-GAL4* and *pdfr(B)-GAL4* (Im and Taghert, 2010), *GMR56H10-GAL4* (Sun et al., 2017), *GMR69F08-GAL4* (Liu et al., 2016); split-GAL4 lines: GMR_MB122B and GMR_SS00681 (Liang et al., 2017), GMR_SS002769 (Robie et al., 2017); *cry-LexA* (Liang et al., 2017), *pdf-LexA* (Shang et al., 2008), *TH-LexA* (Berry et al., 2015); *TH-Flp* (Xie et al., 2018); *UAS-SGG* (Martinek et al., 2001), *UAS-P2X2* and *LexAop-P2X2* (Yao et al., 2012), *LexAop-jGECO1a* (Dana et al., 2016), *UAS-GCaMP6s* and *LexAop-GCaMP6s* (Chen et al., 2013), *UAS-GRAB$_{DA4.4}$* (Sun et al., 2018), *UAS-DopR1-miRNA* and *UAS-DopR2-miRNA* (Liu et al., 2017), *UAS-D2R-miRNA* and *UAS-DopEcR-miRNA* (Xie et al., 2018); *per^{01}* (Konopka and Benzer, 1971), *norpA^{P24}* (Ostroy and Pak, 1974), and *pdfr^{han5403}* (Hyun et al., 2005). *UAS-(FRT.stop)-TeTn* (BL67690), *GMR19C08-LexA* (BL52543), *GMR56H10-GAL4* (BL61644), and *GMR92G05-GAL4* (BL48416) were obtained from Bloomington Stock Center. The *cry-LexA* line was a gift from Dr. F Rouyer (CNRS Gyf, Paris).

All transgenic lines were either generated in the *w1118* (iso31) background or backcrossed more than 4 generations into this background. For mutant flies, *per^{01}*, *norpA^{P24}*, and *pdfr^{han5403}*, the phenotypes of behavioral rhythms and circadian pacemaker neural activity rhythms were measured to help interpret EB-RN neural activity rhythms.

METHOD DETAILS

Nomenclature

The nomenclature of ellipsoid body (EB) subgroups in this study follows Renn et al. (1999a), which was revised by Omoto et al. (2017) reflecting the introduction of more specific driver lines. The EB subgroup labeled by *cry-lexA* and *GMR69F08-GAL4* (also see Liu et al., 2016) was called R2, they were re-named R5 by Omoto et al. (2017). The EB subgroup labeled by *GMR19C08(pdfr)-lexA* was called R4, they were re-named R2 by Omoto et al. (2017).

In vivo fly preparations

The surgical procedure for *Drosophila in vivo* calcium imaging followed methods described in Liang et al. (2016, 2017). Following CO_2 anesthetization, flies were mounted by inserting the neck into a narrow cut in an aluminum foil base. Thus, the foil permitted immersion of the head by saline during preparatory surgery and *in vivo* imaging, while the body remained in an air-filled enclosure. To access circadian pacemaker neurons on one side of the head, a single antenna, a portion of the dorso-anterior head capsule, and a small part of one compound eye were removed from the side ipsilateral to imaging. To access EB-RNs, both antennae and a portion of the dorso-anterior head capsule were removed, while the compound eyes remained intact. The entire surgery was typically ~15 min in duration. For experiments that entailed transection of connectives, or removal of the entire body, the surgery was conducted with fine forceps prior to brain-exposing surgery. The wounds were then closed by application of a bio-compatible silicone adhesive (Kwik-Sil, WPI, USA).

In vivo calcium imaging

Imaging was conducted with custom Objective Coupled Planar Illumination (OCPI) microscopes (Holekamp et al., 2008), as described in Liang et al. (2016, 2017). Briefly, OCPI uses a cylindrical lens to generate a ~5μm thick light sheet, which was coupled to the focal plane of the objective. For 24-hr imaging, the objective coupled light sheet was scanned across the fly brain through the cranial window every 10 min to capture stacks of images. Each stack contained 20 to 40 separate images with a step size of 5 to 10 microns. For each image, exposure time was not more than 0.1 s. During 24-hr imaging, fresh hemolymph-like saline (HL3; 5 mM KCl, 1.5 mM CaCl2, 70 mM NaCl, 20 mM MgCl2, 10 mM NaHCO3, 5 mM trehalose, 115 mM sucrose, and 5 mM HEPES; pH 7.1) was perfused continuously (0.1-0.2 mL/min). Light-dark cycle stimulation during *in vivo* calcium imaging was delivered using a white Rebel LED (Luxeon) controlled by an Arduino UNO board (Smart Projects, Italy) as described in Liang et al. (2017). High-frequency imaging was conducted with a speed-optimized OCPI microscope (Greer and Holy, 2018). Image stacks were captured every 10 s (Figures S5A and S6E), every 2 s (Figures 4A, 7A–7C, and S5B–S5F), or every 1 s (Figures 5C–5F, S3G, and S6D). For each image, exposure time was not more than 0.04 s. For pharmacological tests, each fly was treated once. After 1 or 5-min baseline recordings, 1mL of 0.1 mM PDF solution, 1 mM dopamine solution, or 10 mM ATP solution (pH adjusted to 7) was manually added to a 9 mL static HL3 bath over a ~2 s period. PDF was purchased from Neo-MPS (San Diego, CA, USA) at a purity of 86%.

Cameleon-based calcium imaging

For Figure S2C, FRET imaging was performed as described in Liang et al., (2016). At certain ZTs, living brains were dissected and imaged with an Epifluorescent Olympus BX61 microscope. Exposure times were 20 ms for YFP - FRET and 500 ms for CFP donor. For each ZT point, the ratio values of YFP over CFP were collected from at least 45 cells that were found in at least 5 brains.

In vivo dopamine imaging

Dopamine imaging was conducted following the same procedure as *in vivo* calcium imaging using the OCPI microscope. The dopamine sensor $GRAB_{DA2m}$ is derived from DA1m (Sun et al., 2018), but contains additional point mutations in the inserted cpEGFP. These mutations significantly increase dF/F ~3 fold comparing with DA1m.

Locomotor monitoring during imaging

During 24-hr *in vivo* calcium imaging, *Drosophila* locomotor activity was measured by an infrared detector (LTE-301)/emitter (940nm, LTE-302) circuit. The infrared emitter was aimed toward the body of the fly and the detector received the infrared light transmitted through the fly (shown in Figure 2A). Both the body and leg movements can cause changes in transmitted light intensity. The analog signal from the infrared detector was transmitted through an Arduino UNO board with 100Hz sampling rate. The infrared emitter was shut off for 10 s every 10 min, allowing the microscope to acquire complete volume brain scans. The daily fly locomotor activity pattern was then calculated by counting the activity events within each 10-min bin. The activity events were identified by time-points when the infrared detector signal was out of the range for standard deviation by 3-fold. Then the normalized event count trace was aligned with the EB-R2 neuron calcium signal of the same fly (Figure 2C). The Pearson's correlation coefficient between these two signals was calculated. To test their correlation at an hourly timescale, these two signals then were averaged by a method similar to spike-triggered averaging. 4-hr windows (1 hr before and 3 hr after the trigger point) of calcium signals were aligned by the local maximum (increasing phase) or local minimum (decreasing phase) of calcium signal derivatives. The locomotor signals occurring in these 4-hr windows were then averaged. Analysis was performed using R 3.3.3.

Locomotor activity

To examine the circadian rhythms of locomotor activity, individual flies was monitored using Trikinetics *Drosophila* Activity Monitor (DAM) system for 6 days under light-dark (LD) cycles and then for 9 days under constant darkness (DD) condition. χ^2 periodogram with a 95% confidence cutoff and SNR analysis were used to measure circadian rhythmicity and periodicity (Levine et al., 2002). Arrhythmicity were defined by a power value (χ^2 power at best period) less than 10, width lower than 1, a period less than 18 hr or more than 30 hr. To find the phases of morning and evening peaks, each 24-hr day was split into two halves. For LD, it was split at ZT6. For DD1, it was split at the time of the manually selected midday ''siesta''. Then the morning peak and evening peak were then determined by the maximum activity in each half.

Immunocytochemistry

Immunostaining for PER and beta-Gal followed previous descriptions (Liang et al., 2016). Briefly, fly brains were dissected in ice-cold, calcium-free saline and fixed for 15 m in 4% paraformaldehyde containing 7% picric acid (v/v) in PBS. Primary antibodies included rabbit anti-PER (1:5000; kindly provided by Dr. M. Rosbash, Brandeis Univ.; Stanewsky et al., 1997) and mouse anti-beta-galactosidase (1:1000; Promega, Madison, WI, Cat. #Z3781, Lot #149211). Secondary antisera were Cy3-conjugated (1:1000; Jackson Immunoresearch, West Grove, PA). Images were acquired on the Olympus FV1200 confocal microscope. PER protein immunostaining intensity was measured in ImageJ-based Fiji (Schindelin et al., 2012).

Data reporting

No statistical methods were used to predetermine sample sizes. The selection of flies from vials for imaging and behavioral tests were randomized. The investigators were not blinded to fly genotypes.

QUANTIFICATION AND STATISTICAL ANALYSIS

Imaging data analysis

Calcium imaging data analysis was as described previously (Liang et al., 2016, 2017). Images were acquired by a custom software, Imagine (Holekamp et al., 2008) and processed in Julia 0.6 including non-rigid registration, alignment and maximal projection along z axis. Then ImageJ-based Fiji was used for rigid registration and to manually select regions of interest (ROIs) over individual cells or groups of cells. Average intensities of ROIs were measured through the time course and divided by average of the whole image to subtract background noise. For spontaneous calcium transients, each time trace was then calculated as $\Delta F/F = (F\text{-}F_{min})/F_{mean}$. The minimal intensity over 24-hr recording was regarded as the baseline intensity in order to average the $\Delta F/F$ across different trials. In these different trials, to avoid the influence of the single-photon imaging preparation and the ambient recording environment, 24-hr recording sessions were randomly begun at different Zeitgeber Times. Consequently, the calcium levels at the first time points (F_0) could be either at the peak, the trough, or in the middle of daily calcium rhythms. In order to compare between different trials, F_{min} was used as the baseline. The ΔF then was divided by F_{mean} rather than F_{min}, because F_{min} (the baseline fluorescence of GCaMP6s) may

be zero (below black level of the camera) during 24-hr recordings. For 24-hr time traces, traces of certain cell type ROIs were first aligned, based on Zeitgeber Time and averaged across different flies. Hartigans' dip test and Silverman's test were used to testify whether the averaged 24-h time traces are unimodal or bimodal (Hartigan and Hartigan, 1985; Silverman, 1981). The phase relationship between traces was estimated by cross-correlation analysis. The 24-hr-clock circular plot of phases reflected both mean peak time and phase relationships of the same cell-group traces from different flies. For neurons with daily bimodal patterns (EB-RNs and PPM3-EB DA neurons), each trace was split into two parts: ZT18-ZT6 (morning) and ZT6-ZT18 (evening) to estimate the morning and evening peak phases respectively. For dual-color imaging traces, all signals were filtered (high-pass, 1/30 Hz). To 'spike'-triggered average simultaneous traces of three cell types (Figure 5DE), the peaks of selected cell-type signal were identified by the local maximum of that signal after a low-pass filter (0.2Hz). Unfiltered signals of three cell types were then aligned by these peaks to calculate the averaged traces for individual cell types. For pharmacological calcium responses, each time trace was normalized by the initial intensity (F/F_0). The maximum change was calculated by the maximum difference of normalized intensities between baseline and after drug application. The latency (onset time constant) was calculated by the duration from drug application to the time when the trace reached 63.2% of maximum change. The parametric or nonparametric tests were selected based on F variance tests. All statistics tests are two-sided. All the sample size information (n values and what the n represents), as well as specific statistical methods, are listed in corresponding figure legends. Trace analysis and statistics were performed using R 3.3.3 and Prism 7 (GraphPad, San Diego CA).

Neuron, Volume *102*

Supplemental Information

Morning and Evening Circadian Pacemakers Independently Drive Premotor Centers via a Specific Dopamine Relay

Xitong Liang, Margaret C.W. Ho, Yajun Zhang, Yulong Li, Mark N. Wu, Timothy E. Holy, and Paul H. Taghert

Figure S1

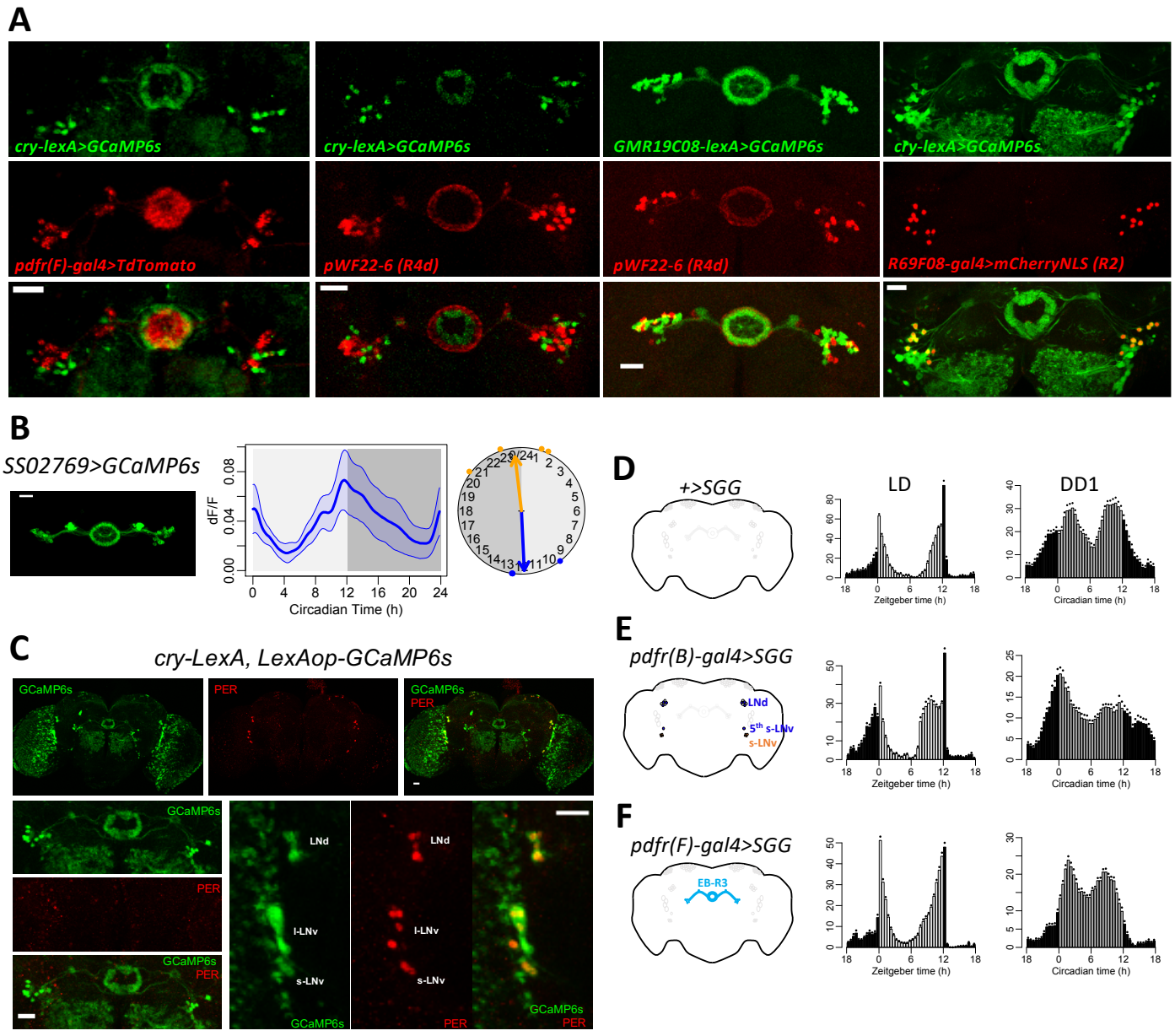

Figure S1. The different subgroups of ellipsoid body (EB) ring neurons do not display circadian pacemaker cell properties. Related to Figure 1.

(**A**) Confocal images of different subgroups of EB ring with different concentric arborization radii featured by different genetic drivers: the *cry-LexA* pattern did not overlap with that the *pdfr(F)-GAL4 pattern*; the *cry-LexA* pattern did not overlap with the *pWF22-6* pattern (R4d subgroup, see 30); the *GMR19C08(pdfr)-lexA* pattern did not overlap with the pattern of *pWF22-6*; the *cry-LexA* pattern did overlap with the that of *GMR69F08-GAL4* (R2 subgroup, see 69); Scale bars, 20 µm.

(**B**) Daily Ca^{2+} activity patterns of the EB-RN subgroup R4, labelled by split-GAL4 drivers which caused the strongest effect on increasing locomotor activity (18).

(**C**) Immunostaining of PER protein in the *cry-LexA, LexAop-GCaMP6s* fly at ZT0. Scale bars, 20 µm. PER can be detected in circadian pacemaker neurons, but not in EB-RNs.

(**D-F**) Average locomotor activity of (D) wild type (*UAS-sgg*, n = 16 flies), (E) flies with Shaggy (SGG) expressed in s-LNv and three out of the six LNd with *pdfr(B)-GAL4* (n = 16 flies), and (F) flies with SGG expressed in EB-R3 neurons with *pdfr(F)-GAL4* (n = 32 flies) under LD cycles and in the first day under DD (DD1). Accelerating molecular clocks in M and E cells (E) advanced both morning and evening behavioral phases, yet SGG over-expression in EB-RN neurons (F) was inconsequential.

Figure S2

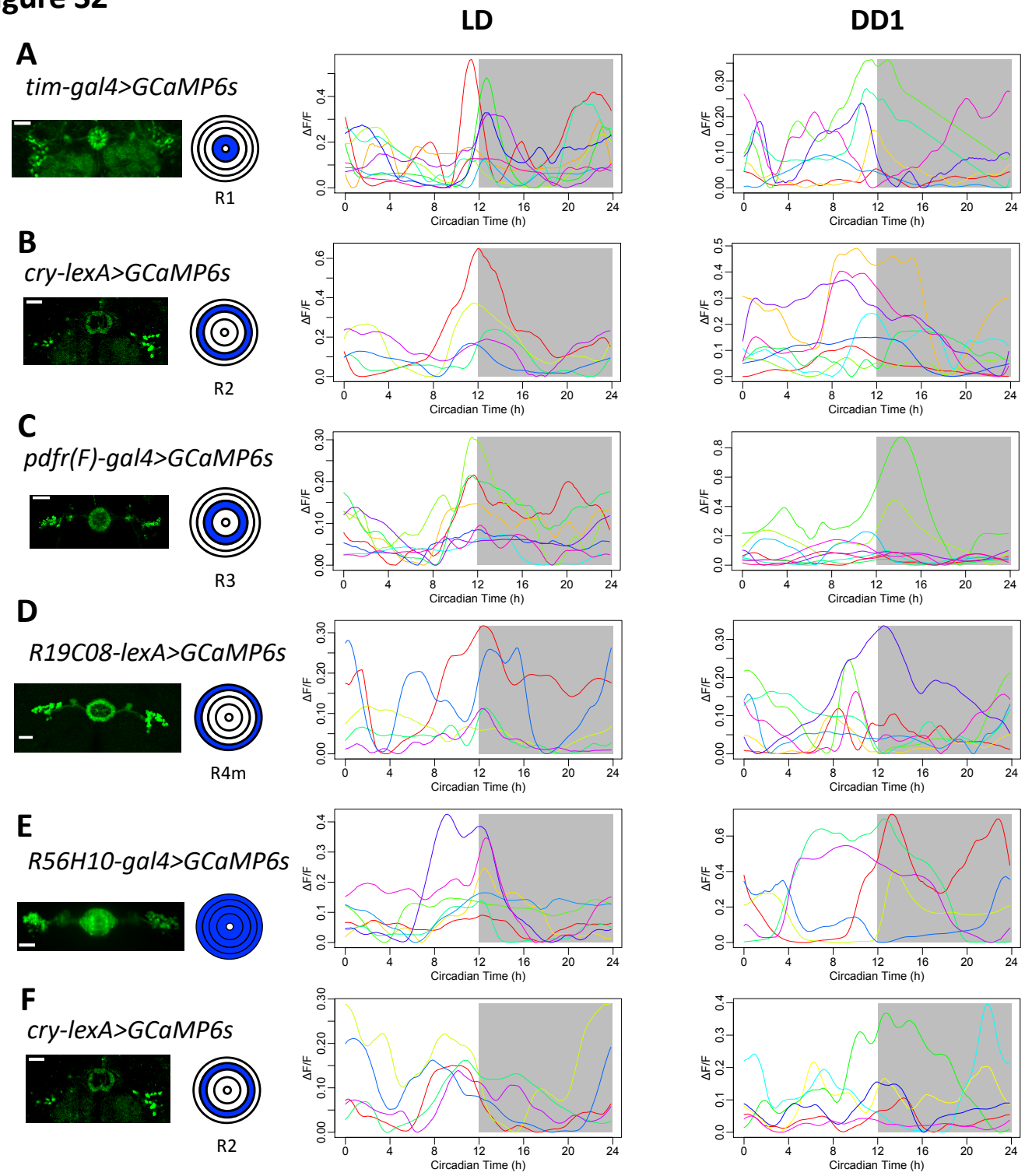

Figure S2. Daily Ca^{2+} activity patterns of the EB ring neuron subgroups under LD and DD. Activity traces of individual flies are plotted in different colors. Related to Figure 1.

(A) EB-R1 neurons labelled by *tim-GAL4.*

(B) EB-R2 neurons labelled by *cry-lexA.*

(C) EB-R3 neurons labelled by *pdfr(F)-GAL4.*

(D) EB-R4 neurons labelled by *R19H08(pdfr)-lexA.*

(E) EB-R1-4 neurons labelled by *R56H10-GAL4*.

(F) EB-R2 neurons labelled by *cry-lexA* measured in Figure 2.

Figure S3

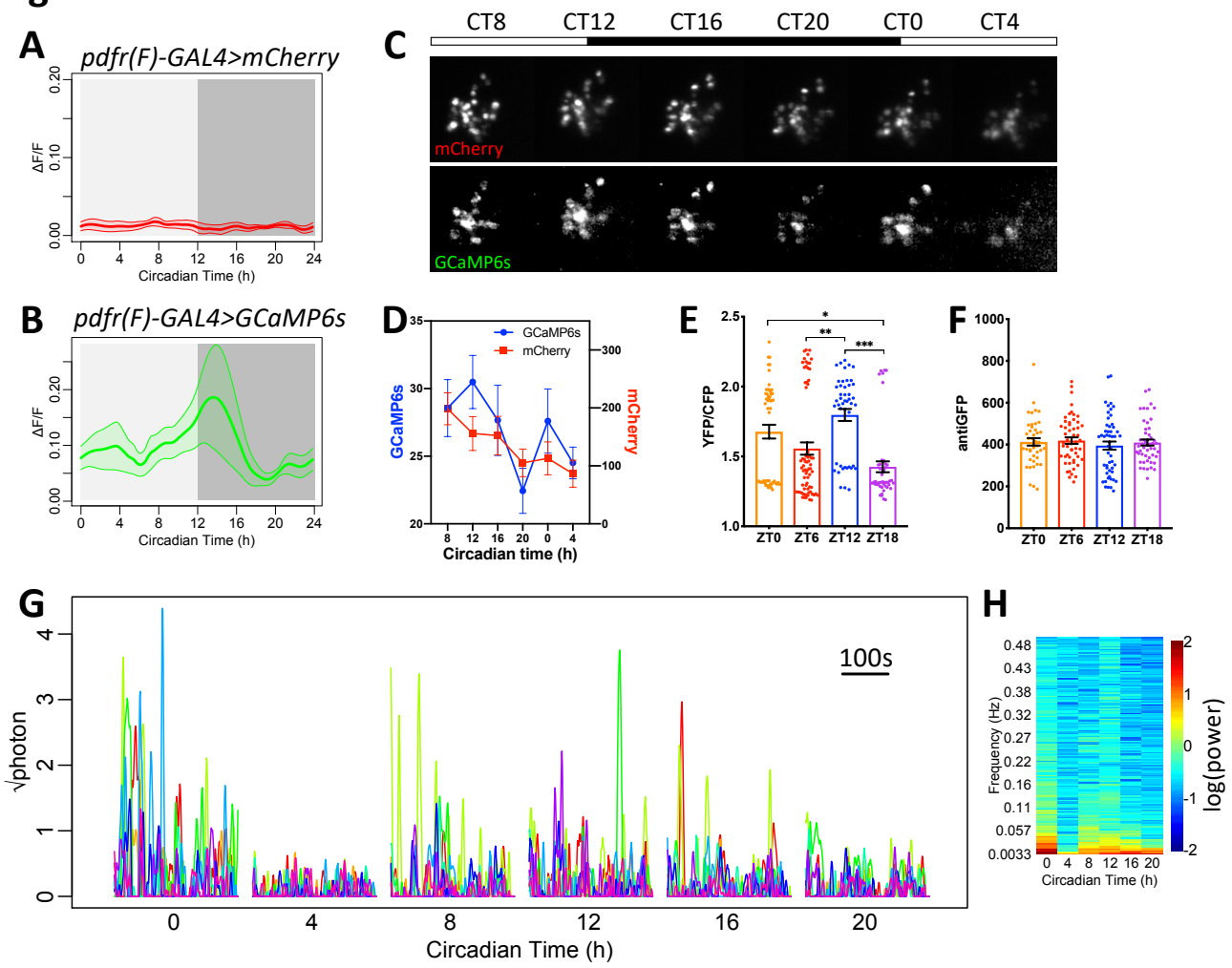

Figure S3. Daily bimodal neural activity patterns of EB ring neurons. Related to Figure 1.

(**A**) 24-hr fluorescence changes of stable red fluorescent protein (mCherry) whose fluorescence is not changed with calcium expressed in EB-R3 driven by *pdfr(F)-gal4*.

(**B**) 24-hr fluorescence changes of calcium sensor GCaMP6s expressed in EB-R3 driven by *pdfr(F)-gal4* (replotted from Figure 1F - right panel).

(**C**) Representative images of ER-R3 neuron mCherry and GCaMP6s fluorescence in a *pdfr(F)-gal4>GCaMP6s,mCherry.NLS* fly at six different time points over 24-hr day.

(**D**) Averaged fluorescence intensity in (C). Error bars denote SEM.

(**E**) Quantification of EB-RN calcium levels at four distinct time points, revealed by ratiometric FRET-based Cameleon2.1 imaging. The ratio of YFP and CFP signals were significantly higher at ZT0 and ZT12 than ZT6 and ZT18 in of EB-R1 labelled by *tim-gal4* (*P < 0.05, **P < 0.01, ***P < 0.001, Kruskal-Wallis test followed by post hoc Dunn's tests).

(**F**) Expression levels of GCaMP6s revealed by immunostaining with anti-GFP antibody in EB-R2 neurons driven by *cry-LexA* were stable over four times of day (P = 0.7586, Kruskal-Wallis test).

(**G**) Raw calcium activity traces of EB-R3 neurons (labelled by *pdfr(F)-gal4*) from one representative fly at six different time points over 24-hr day. For each time point, calcium activity was recorded at 1Hz for 5 min. Individual neurons were color-coded. The calcium signal was calculated as the square root of photon number collected from an individual region of interest, representing fold changes over the standard deviation of the shot noise.

(**H**) Daily pattern of the power spectrum over the 5-min recording session at each of 6 timepoints.

Figure S4

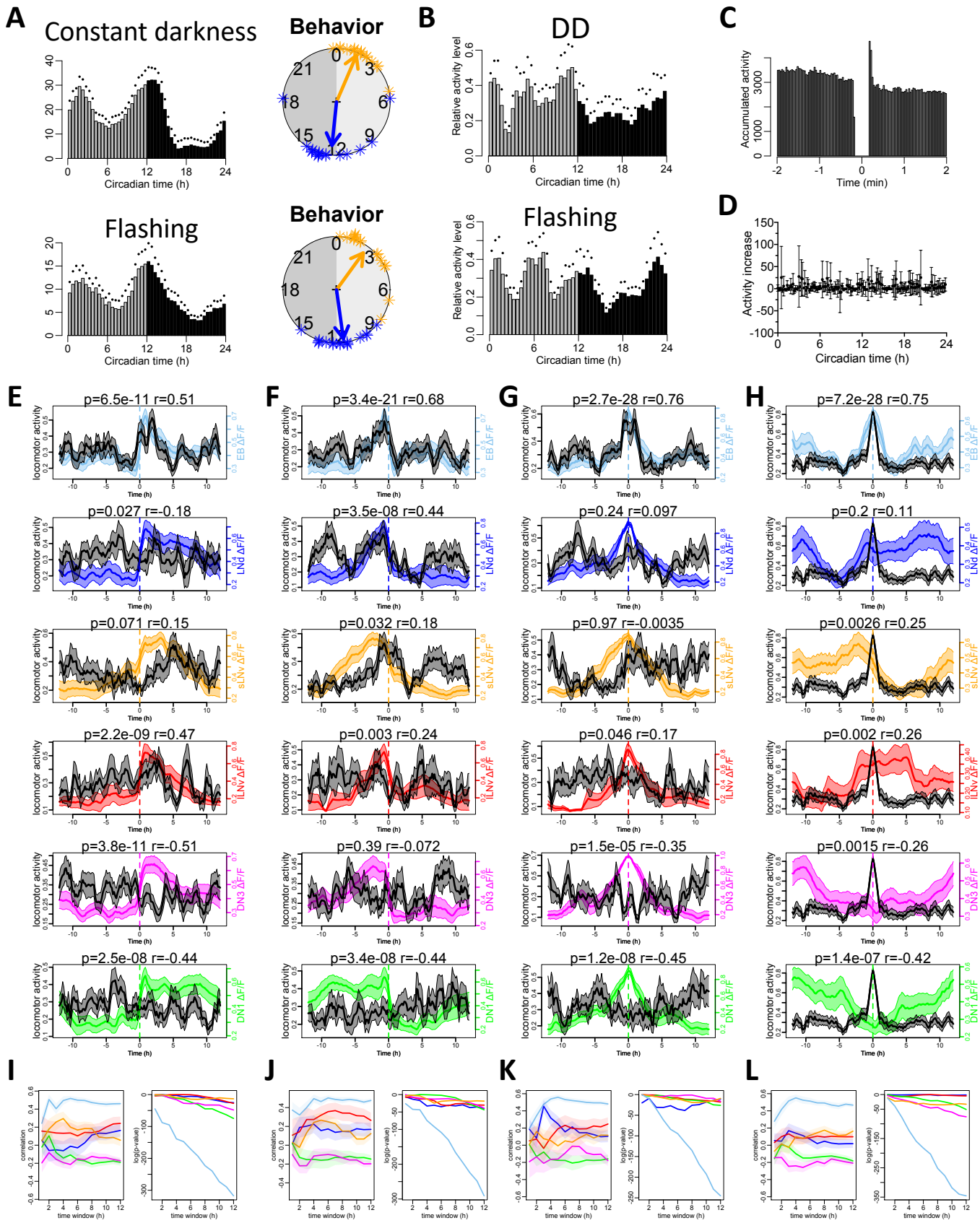
A
Constant darkness
Behavior
Flashing
Behavior
B
DD
Flashing
C
D
Circadian time (h)
Time (min)
Relative activity level
Accumulated activity
Activity increase
E
F
G
H
p=6.5e-11 r=0.51
p=3.4e-21 r=0.68
p=2.7e-28 r=0.76
p=7.2e-28 r=0.75
p=0.027 r=-0.18
p=3.5e-08 r=0.44
p=0.24 r=0.097
p=0.2 r=0.11
p=0.071 r=0.15
p=0.032 r=0.18
p=0.97 r=-0.0035
p=0.0026 r=0.25
p=2.2e-09 r=0.47
p=0.003 r=0.24
p=0.046 r=0.17
p=0.002 r=0.26
p=3.8e-11 r=-0.51
p=0.39 r=-0.072
p=1.5e-05 r=-0.35
p=0.0015 r=-0.26
p=2.5e-08 r=-0.44
p=3.4e-08 r=-0.44
p=1.2e-08 r=-0.45
p=1.4e-07 r=-0.42
locomotor activity
EB ΔF/F
LNd ΔF/F
sLNv ΔF/F
lLNv ΔF/F
DN3 ΔF/F
DN1 ΔF/F
Time (h)
I
J
K
L
correlation
log(p-value)
time window (h)

Figure S4. Correlation between daily locomotor activity and neural activity. Related to Figure 2.

(A) Average locomotor activity and phase distribution of wild type flies (*tim-gal4>GCaMP6s*) in the first day under constant darkness (above) without and (below) with a blue light flashing by the side at the comparable frequency and intensity as light-sheet scanning (n = 16 in each condition). The fly behavior was measured by Trikinetics *Drosophila* Activity Monitor (DAM) system.

(B) Average locomotor activity of wild type flies (*cry-lexA>GCaMP6s*) in the first day under constant darkness (above) without and (below) with light-sheet calcium imaging every 10 min. The fly behavior was measured by the setup shown in Figure 2A (n = 6 in each condition).

(C) From the data in lower panel of (B), locomotor activity was elevated for the first 2 sec after each light-sheet scanning. 4-min activity records in 1Hz sampling rate were aligned at the time light-sheet scanning (time 0). The behavior monitor was shut off for 10 sec during light-sheet scanning.

(D) Daily pattern of locomotor activity difference triggered by light-sheet scanning as a function of time of day. The y-axis represents the difference in locomotor activity $activity_{post}$ - $activity_{pre}$, where each is measured in a 5 sec block. The instantaneous increase in locomotor activity triggered by light-sheet scanning did not depend on time of day.

(E) Average locomotor activity (black) and Ca^{2+} activity (colors) aligned by increasing phase of Ca^{2+} activity in EB-R2 and in different groups of circadian neurons.

(F) Average locomotor activity (black) and Ca^{2+} activity (colors) aligned by decreasing phase of Ca^{2+} activity.

(G) Average locomotor activity (black) and Ca^{2+} activity (colors) aligned by the peak of Ca^{2+} activity.

(H) Average Ca^{2+} activity (colors) in EB-R2 and different groups of circadian neurons aligned by the peak of locomotor activity (black).

(**I-L**) Averaged (left) correlation coefficient and (right) p-value between neural activity and behavior measurements within different time windows (number of hours before and after the trigger point) aligned by different ways as in (E-H). Different groups of neurons were colored coded. Neural activity of EB-RNs (light blue) shows stronger correlation with behavior than circadian neurons.

Figure S5

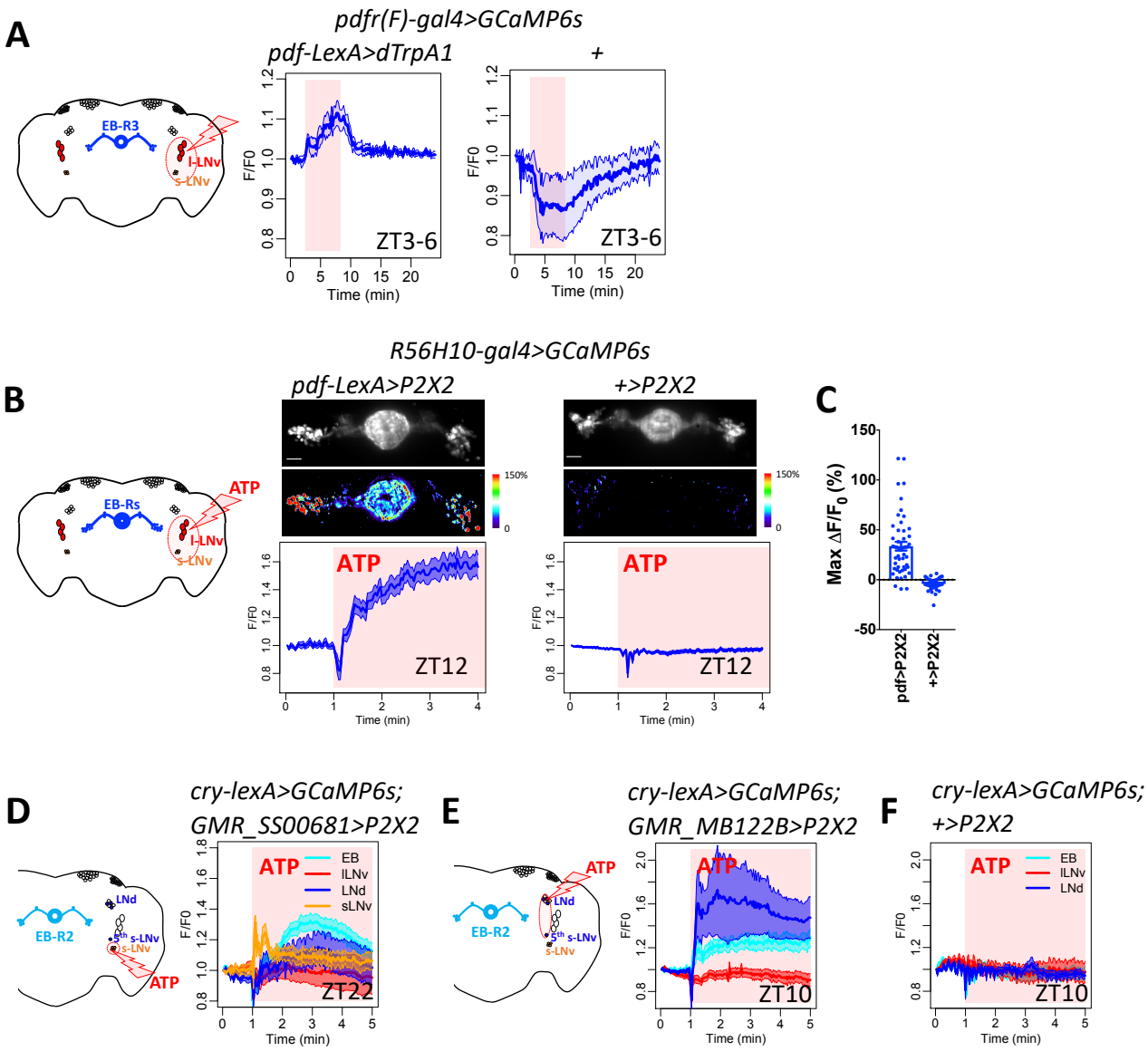

Figure S5. EB-RNs respond to circadian neuron activation. Related to Figure 4.

(**A**) Left, map of EB-RNs and circadian pacemaker neurons. Right, average traces of EB-R3 neurons responding to increase of temperature in flies with dTrpA1 expressed in PDF neurons (red, n = 7 flies) and in control flies without dTrpA1 expression (blue, n = 4 flies). Red shading indicates duration of temperature increase.

(**B**) Responses of EB-RNs labelled by *R56H10-GAL4* to ATP application in flies with P2X2 expressed in PDF neurons, both s- and l-LNv (left, n = 5 flies) and in control flies without P2X2 expression (right, n = 3 flies). Red aspect indicates duration of ATP application. Above, example image baseline Ca^{2+} signal and maximum Ca^{2+} signal changes. Below, average traces of EB ring neurons.

(**C**) Maximum Ca^{2+} signal changes within 3 min after ATP application in individual EB-RNs in (B).

(**D**) Responses of EB-R2 neurons, and circadian pacemaker neurons labelled by *cry-LexA,* to ATP application in flies with P2X2 expressed in s-LNv (n = 6 flies).

(**E**) Responses of EB-R2 neurons and circadian pacemaker neurons labelled by *cry-LexA* to ATP application in flies with P2X2 expressed in E cells: three LNd and the 5th s-LNv neurons (n = 5 flies).

(**F**) Responses of EB-R2 neurons, and circadian pacemaker neurons labelled by *cry-LexA,* to ATP application in flies in *UAS* control flies, i.e., without P2X2 expression (n = 3 flies).

Figure S6

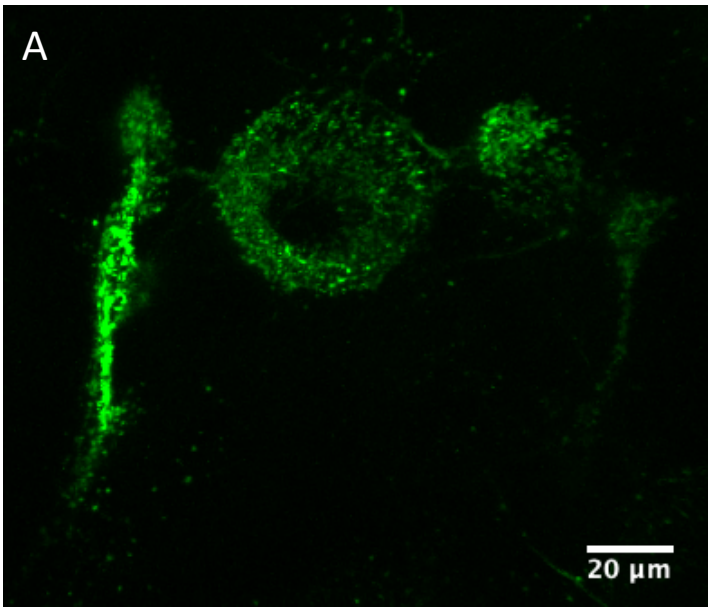
A
20 µm

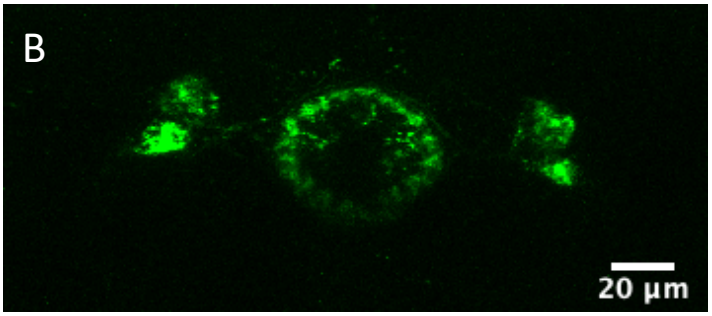
B
20 µm

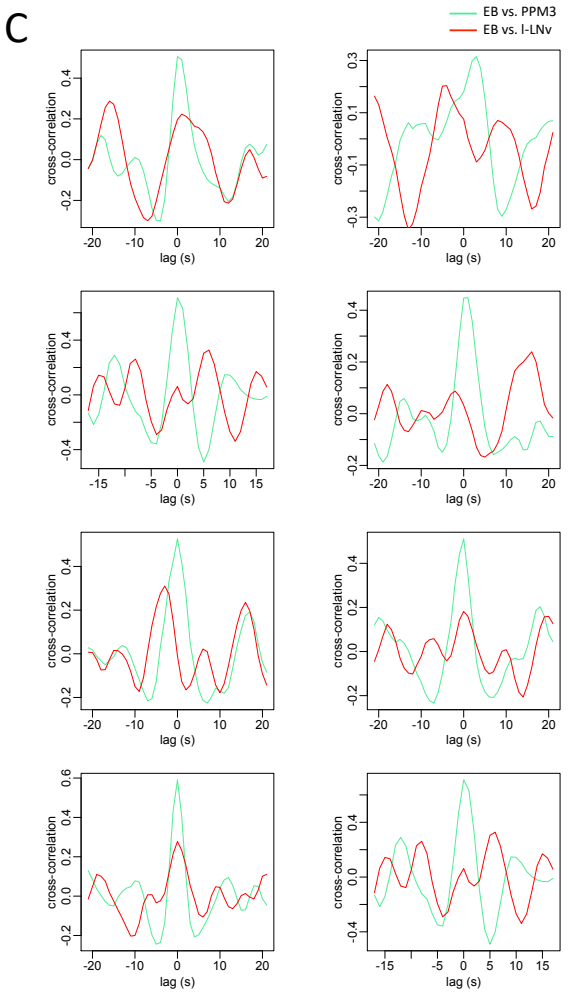
C
EB vs. PPM3
EB vs. l-LNv
cross-correlation
lag (s)

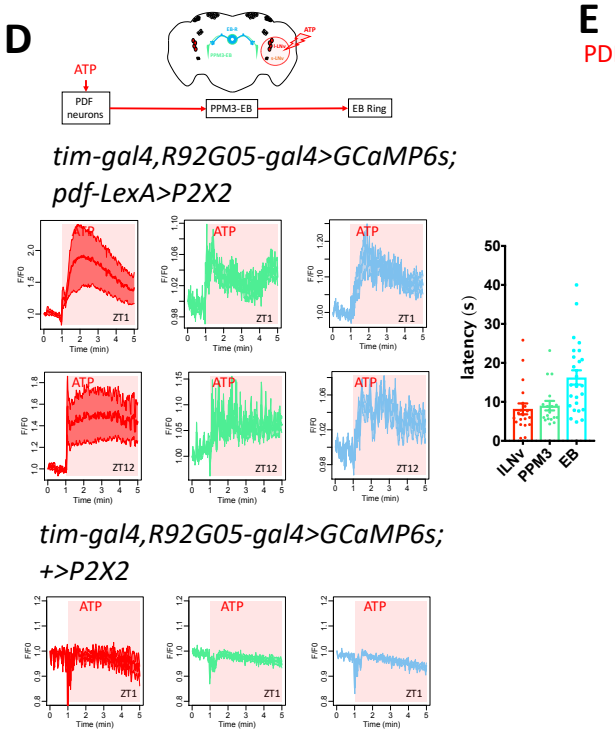
D
ATP
PDF neurons
PPM3-EB
EB Ring
tim-gal4,R92G05-gal4>GCaMP6s; pdf-LexA>P2X2
ATP
ZT1
ZT12
F/F0
Time (min)
latency (s)
ILNv
PPM3
EB
tim-gal4,R92G05-gal4>GCaMP6s; +>P2X2

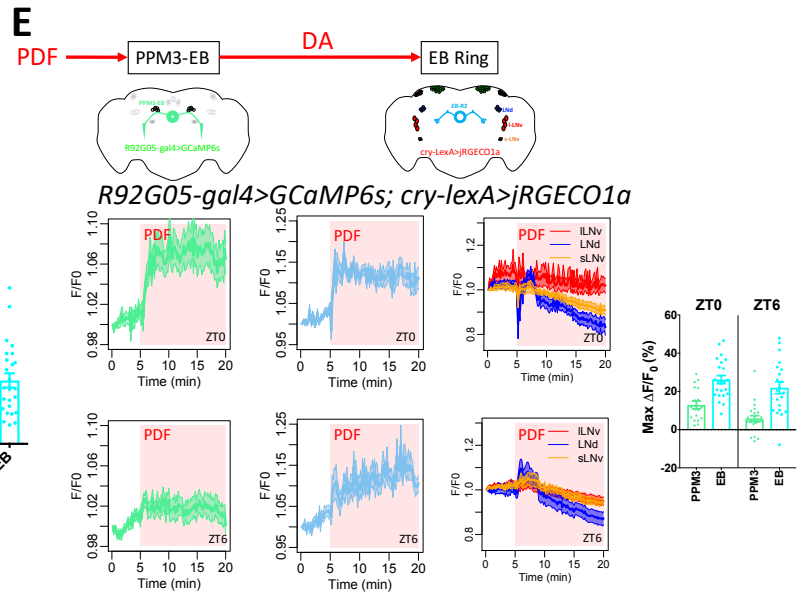
E
PDF
PPM3-EB
DA
EB Ring
R92G05-gal4>GCaMP6s
cry-LexA>jRGECO1a
R92G05-gal4>GCaMP6s; cry-lexA>jRGECO1a
PDF
ZT0
ZT6
ILNv
LNd
sLNv
Time (min)
Max ΔF/F0 (%)
PPM3
EB

Figure S6. Tests of connections from PDF neurons to PPM3-EB and to EB-RNs. Related to Figure 5.
(A) *TH-LexA,LexAop-GFP11; R92G05-GAL4/UAS-GFP1-10* brain visualized for GFP in the entire processes of PPM3-EB neurons.
(B) GRASP analysis reveals synaptic connections between EB-RNs and PPM3-EB. *R56H10-LexA,LexAop-GFP11; R92G05-GAL4/UAS-GFP1-10* brain visualized for GFP in the synapses between EB-RNs and PPM3-EB neurons.
(C) Cross-correlograms for eight individual flies from Figure 5B-F. Spontaneous calcium activity shows higher correlation between PPM3-EB and EB-RNs (green) than that between PPM3-EB and l-LNv (red).
(**D**) Above, map of PPM3-EB DA neurons, EB-RNs, and circadian pacemaker neurons. Below-left, average traces of PDF neurons, PPM3-EB neurons, and EB-R1 neurons responding to activation of P2X2-expressing PDF neurons by ATP at two zeitgeber time points: ZT1 (n = 5 flies) and ZT12 (n = 4 flies). Below-middle, response latency (onset time constant) of EB-RNs is longer than that of PPM3-EB neurons (p=0.0029, Mann-Whitney test). below-right, average traces of PDF neurons, PPM3-EB neurons, and EB-R1 neurons responding to bath application of ATP to *LexAop-P2X2*-only control flies at ZT1 (n = 5 flies).
(**E**) As in Figure 5B-F, dual-color Ca^{2+} imaging: GCaMP6s in PPM3-EB and jRGECO1a in EB-R2 and circadian pacemaker neurons. Below-left, average traces of PPM3-EB neurons, EB-R2 neurons, and circadian pacemaker neurons responding to the bath-application of neuropeptide PDF (10^{-5} M) at two zeitgeber time points: ZT0 (n = 3 flies) and ZT6 (n = 3 flies). Below-right, maximum Ca^{2+} signal changes in individual cells after PDF bath application.

Figure S7

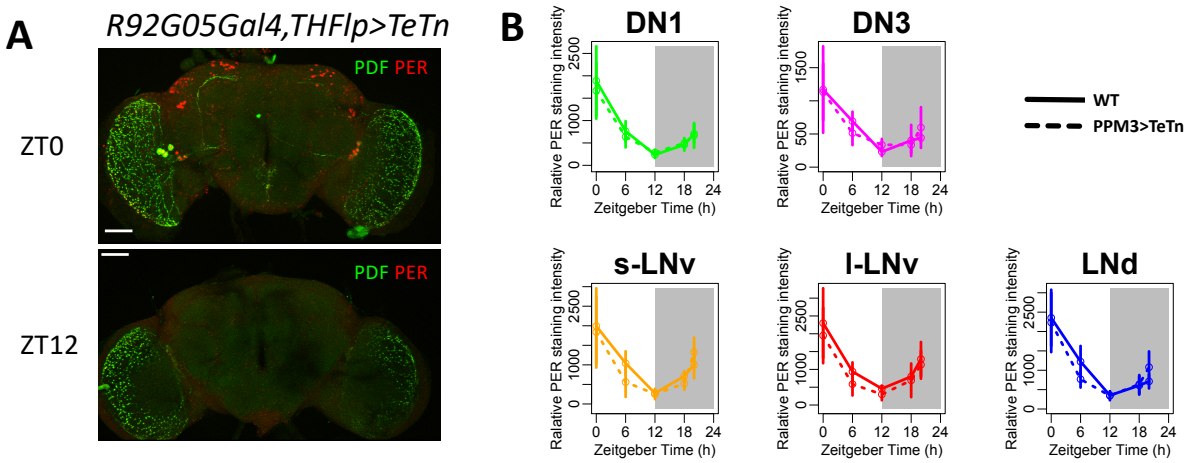

Figure S7. PER protein rhythms of control flies and flies expressing tetanus toxin (TeTn) in PPM3-EB neurons in Figure 6A. Related to Figure 6.

(**A**) Representative images of immunostaining against PDF and PER at two different time points: ZT0 and ZT12 of flies expressing TeTn in PPM3-EB.

(**B**) Quantification of PER protein staining intensity at five different time points in five groups of circadian neurons from control flies and flies expressing TeTn in PPM3-EB (n > 3 flies for each time points).

Table S1

Manipulation of dopamine signal and EB-RNs impair circadian locomotor activity rhythms.
Related to Figure 1 & 6.
AR, arrhythmic. Period and power are calculated by χ2 periodogram. Activity represents averaged activity count per 30 min.

Genotype	N	AR	Period (h)	SEM	Power	SEM	Activity	SEM
R56H10-GAL4>+	15	7%	23.50	0.10	88.36	10.97	20.53	2.27
+>UAS-TeTn	16	0%	24.13	0.08	98.29	11.81	20.60	1.91
R56H10-GAL4>UAS-TeTn	14	64%	24.00	0.97	10.69	3.12	6.07	1.25
TH-Flp/+; R92G05-GAL4/+	16	0%	23.23	0.12	71.07	7.84	15.69	1.58
UAS-(FRT.stop)-TeTn/+;	22	9%	23.52	0.12	38.13	7.42	17.50	2.62
TH-Flp/UAS-(FRT.stop)-TeTn;	21	24%	23.17	0.12	22.15	5.01	15.43	1.57
TH-Flp/UAS-(FRT.stop)-TeTn; R92G05-GAL4/+	24	83%	23.64	0.05	3.03	1.58	13.85	4.46
R56H10-GAL4>+	39	5%	23.38	0.05	82.68	9.20	16.80	1.36
+>DopR1-miRNA	12	0%	23.42	0.08	124.06	14.01	17.70	0.95
R56H10-GAL4>DopR1-miRNA	32	3%	23.63	0.05	84.18	8.57	22.21	1.22
+>DopR2-miRNA	16	0%	23.75	0.07	147.40	10.73	24.70	2.56
R56H10-GAL4>DopR2-miRNA	15	20%	23.56	0.10	33.15	7.17	22.38	1.75
+>D2R-miRNA	23	0%	23.76	0.09	72.97	9.89	23.30	2.00
R56H10-GAL4>D2R-miRNA	25	12%	23.50	0.10	26.53	4.24	9.41	1.12
+>DopEcR-miRNA	15	0%	23.95	0.13	93.91	12.93	21.50	1.43
R56H10-GAL4>DopEcR-miRNA	15	7%	23.57	0.07	72.89	5.54	19.60	1.97

Table S2

List of driver/ reporter lines used in this study. Related to Figure 1, 4, 5, S1, & S2.
The nomenclature of ellipsoid body ring neuron (EB-RN) subgroups used in this study – different from that in Omoto et al. (2017) - are here indicated.

Driver / Reporter Lines	EB-RN subgroup	EB-RN subgroup nomenclature by Omoto et al. (2017)	other cell types
tim(UAS)-GAL4	R1	R1	All circadian pacemaker neurons and others
pdfr(F)-GAL4	R3	R3	N/A
cry-LexA	R2	R5	CRY-positive circadian pacemaker neurons and others
GMR69F08-GAL4	R2	R5	N/A*
GMR_SS002769	R2/R4m	R2	N/A
GMR19C08-LexA	R4m	R2	N/A
GMR56H10-GAL4	R1-4	R1-5	N/A
pWF22-6-lacZ	R4d	R4	N/A
pdfr(B)-GAL4	N/A	N/A	all s-LNv, 3 CRY-positive LNd, and 2 DN1
GMR_SS00681	N/A	N/A	4 PDF-positive s-LNv
GMR_MB122B	N/A	N/A	the 5th s-LNv and 3 CRY-positive LNd
pdf-LexA	N/A	N/A	PDF-positive s-LNv and l-LNv
GMR92G05-GAL4	N/A	N/A	PPM3-EB and others
GMR92G05-GAL4, TH-Flp	N/A	N/A	PPM3-EB

*N/A indicates invisible in the brain